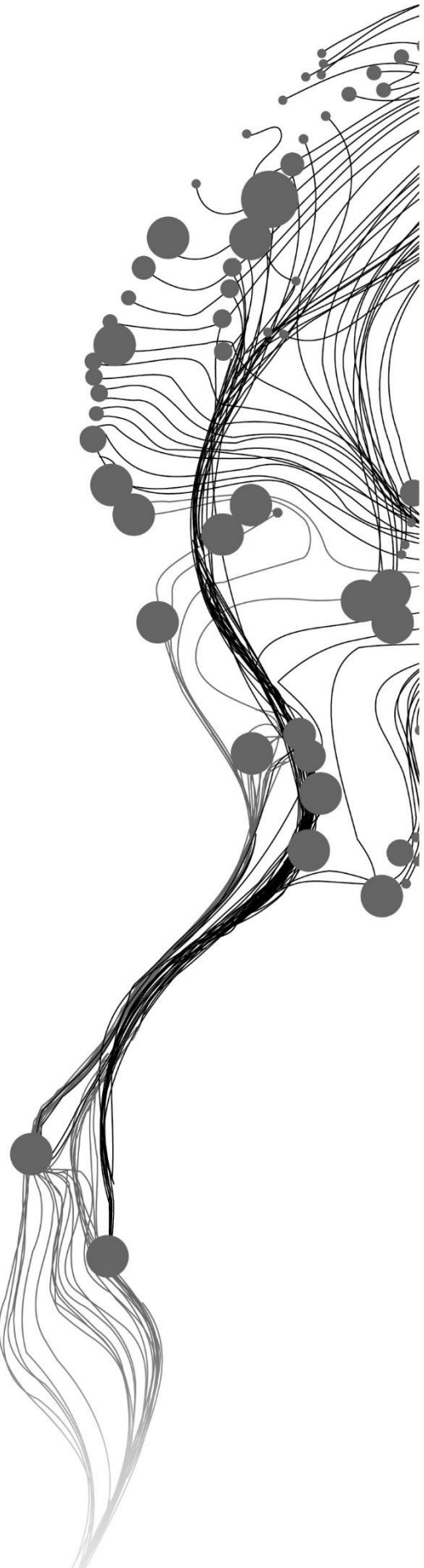


**Assessing the accuracy of UAV-DTM generated under different forest canopy density and its effect on estimation of aboveground carbon in Asubima forest, Ghana**

CLEMENT OBENG-MANU  
FEBRUARY, 2019.

SUPERVISORS:  
ir. L.M. van Leeuwen - de Leeuw  
dr. P. Nyktas





# **Assessing the accuracy of UAV-DTM generated under different forest canopy density and its effect on estimation of aboveground carbon in Asubima forest, Ghana**

CLEMENT OBENG-MANU

Enschede, The Netherlands, February, 2019

Thesis submitted to the Faculty of Geo-Information Science and Earth Observation of the University of Twente in partial fulfilment of the requirements for the degree of Master of Science in Geo-information Science and Earth Observation.  
Specialization: Natural Resources Management

**SUPERVISORS:**

ir. L.M. van Leeuwen - de Leeuw  
dr. P. Nyktas

**THESIS ASSESSMENT BOARD:**

dr. Y.A. Hussin (Chair)  
dr. T.L.U. Kauranne (External Examiner, Lappeenranta University of Technology, Finland)

#### DISCLAIMER

This document describes work undertaken as part of a programme of study at the Faculty of Geo-Information Science and Earth Observation of the University of Twente. All views and opinions expressed therein remain the sole responsibility of the author, and do not necessarily represent those of the Faculty.

## ABSTRACT

The relatively low cost and usefulness of UAV coupled with advances in photogrammetry and computer vision have caused a global rise in the use of UAV for surveying. Images obtained from UAV has been used to derive forest parameters to estimate aboveground biomass and carbon. However, the quality of results obtained from UAV image processing needs further assessment.

The sensors onboard UAV's cannot penetrate forest canopy cover which makes it difficult for UAV to image the forest floor, especially in a dense canopy forest. With the difficulty of UAV mirroring the forest floor, fewer points will be generated on the forest floor, but many points will be generated on top of the forest canopy. With fewer points on the forest floor, poor Digital Terrain Model (DTM) will be generated in contrast to the Digital Surface Model (DSM) created where many points are created and used.

In this study, the quality of DTM generated from UAV images under four canopy density classes (open canopy plantation, medium canopy plantation, dense canopy plantation, and dense riparian forest) and its effect on the estimation of aboveground carbon was assessed. The accuracy of UAV-DTM was assessed by comparing to field point obtained from a Real-Time Kinematic (RTK) survey and calculating the root mean square error. Canopy Height Models (CHM) per canopy density class were developed from the UAV and field point data to estimate tree height. The t-test was used to determine the similarity/difference between tree height estimated from UAV and field point data at 95% confidence interval. Furthermore, manual digitizing was used to extract the crown projection area (CPA) which was used with its associated field measured DBH to develop a mathematical model. The CPA-DBH model developed was used to predict DBH that could not be measured. From the forest parameters (DBH and tree height), an allometric equation and conversion factor were used to estimate aboveground carbon. Aboveground carbon was estimated from both UAV and field point data, and the t-test was used to determine if there is a statistical difference.

From the accuracy assessment, the riparian forest exhibits the highest error. Also, the field point elevation in open, medium, and dense canopy was not different to UAV derived elevation unlike the riparian forest. According to the DBH-CPA model developed, there was a positive relationship between the CPA and DBH. The result of the tree height estimated from UAV and field point shows that there is no significant difference between tree height estimated from UAV and field data for open, medium, and dense canopy density but the tree height estimated from UAV in the riparian forest is significantly different from field point estimated tree height. The t-test for aboveground carbon estimated also shows that there is no statistical difference in UAV and field point estimated aboveground carbon for open, medium, and dense plantation canopy. However, aboveground carbon estimated from UAV and field point data in the riparian forest is statistically different.

In conclusion, forest canopy density influences the estimation of aboveground carbon in the riparian and plantation forests. The difference in the riparian forest is significant while that of the open, medium, and dense canopy plantation is not.

Keywords: aboveground carbon, CHM, CPA, DBH, DTM, DSM, forest canopy density, UAV.

## ACKNOWLEDGEMENTS

My greatest thanks and appreciation is to the Almighty God who has granted me the gift of life and good health throughout my life. Without God, it would not have out been possible to pursue and successfully complete this programme. I thank the International Christian Fellowship (ICF) for creating an atmosphere to reignite my love for God.

I take this opportunity to thank the Netherlands Government and the Netherlands Organization for International Cooperation in Higher Education (NUFFIC) for the scholarship granted that caters for all financial cost making it possible to concentrate on just the academics.

I am grateful and thankful to Ms. ir. L.M. van Leeuwen – de Leeuw and dr. P. Nyktas for their kind heart, patience, encouragement, and advice throughout the research. It was fun working with you both and I learnt a lot.

I am also sincerely grateful to dr. S.J. Zwart, dr. ir. T.A. Groen, L.H. De Oto, dr. Y.A. Hussin, dr. T. Wang for all their effort and time in helping me to further comprehend concepts and idea during the thesis. To dr. I.C. van Duren, I am very grateful for organizing a series of seminar to improve how we write the thesis. To Tim Roberts, am really grateful for taking time to teach me how to pilot the UAV among other things. To the whole staff of the Faculty of Geo-Information Science and Earth Observation (ITC), I thank you for the knowledge I gain throughout my stay.

I would like to extend genuine thanks to the staff and management of Form Ghana and Form International especially Willem Fourie, Abubakari Tahiru, Alex Amoako, Andries Polinder, Tieme Wanders, and Rosa Diemont.

I am grateful for the amazing friends I made at the Faculty of ITC, ICF, and the NRS 2017-2019 group. It was amazing spending 18 months with you guys.

Finally, I am extremely grateful to Clarissa Annan and Aseda Obeng-Manu for the love, patience, advice and for making my stay away from home worthwhile. To my mother, father and siblings, I am also grateful for the love and patience during my absence.

# TABLE OF CONTENTS

---

1.	Introduction .....	1
1.1.	Background.....	1
1.2.	Research problem.....	3
1.3.	Research objectives .....	4
1.4.	Research questions .....	4
1.5.	Research hypothesis.....	5
1.6.	Conceptual diagram .....	5
2.	Study area, materials, and method .....	6
2.1.	Study area.....	6
2.1.1.	Climate.....	6
2.1.2.	Vegetation .....	6
2.2.	Material.....	7
2.3.	Method .....	7
2.4.	Pre-fieldwork.....	8
2.5.	Fieldwork .....	9
2.5.1.	Reconnaissance and canopy density image capture .....	9
2.5.2.	Sampling design .....	9
2.5.3.	UAV mission planning and image acquisition .....	9
2.5.4.	Topographic survey.....	10
2.5.5.	Biometric data collection.....	13
2.6.	Data processing.....	14
2.6.1.	Forest canopy density classification.....	14
2.6.2.	UAV image processing .....	14
2.6.3.	Generating a DTM from field measured points.....	16
2.6.4.	UAV DTM accuracy assessment.....	17
2.6.5.	Canopy height model (CHM) generation .....	18
2.6.6.	Crown projection area (CPA).....	19
2.6.7.	CPA-DBH relation.....	19
2.6.8.	Individual tree height extraction .....	19
2.6.9.	Estimating aboveground carbon.....	20
2.7.	Data analysis .....	20
3.	Results .....	21
3.1.	Biometric data .....	21
3.2.	Field point result.....	22
3.3.	UAV processing result.....	22
3.4.	Accuracy assessment of UAV DTM.....	23
3.5.	Canopy height modeling per UAV block.....	25
3.6.	Crown projection area (CPA).....	26
3.7.	Tree height per canopy density class.....	27
3.8.	Crown projection area (CPA) and diameter at breast height (DBH) relation .....	29
3.9.	Aboveground carbon estimation .....	30
4.	Discussion.....	33
4.1.	Distribution of biometric data (DBH).....	33
4.2.	UAV-DTM accuracy assessment.....	34

4.3.	CPA-DBH relation.....	37
4.4.	Comparison of UAV and field point estimated tree height.....	37
4.5.	Aboveground carbon estimation .....	37
4.6.	Limitations .....	38
5.	Conclusion and recommendation.....	39
5.1.	Conclusion .....	39
5.2.	Recommendation .....	39
6.	Appendices .....	45
	Appendix 1: Field data collection sheet.....	45
	Appendix 2: DBH-CPA models .....	46
	Appendix 3: Python code.....	48



## LIST OF FIGURES

---

Figure 1-1: A series of overlapping photographs as input for structure from motion .....	3
Figure 1-2: Conceptual diagram of system interactions .....	5
Figure 2-1: Map of Asubima forest reserve, Ghana. ....	6
Figure 2-2: Flowchart of the implemented method.....	8
Figure 2-3: UAV blocks in the study area .....	10
Figure 2-4: Location of benchmark, consecutive point (B1 – B6) and desired base station location. ....	12
Figure 2-5: Summary of the GNSS setup.....	12
Figure 2-6: Field points within each UAV block .....	13
Figure 2-7: Forest canopy density image (left), after applying threshold (middle), and calculating the open area in the image (right).....	14
Figure 2-8: Photogrammetric workflow used.....	15
Figure 2-9: Delaunay triangles and the associated DEM.....	16
Figure 2-10: Decrease of weight with distance illustration.....	17
Figure 2-11: Statistics of IDW and TIN interpolation.....	17
Figure 3-1: Histogram and normal distribution curve of measured DBH.....	21
Figure 3-2: DTM generated from field points.....	22
Figure 3-3: UAV result for block 1 .....	22
Figure 3-4: Photogrammetric result for block 2.....	23
Figure 3-5: Q-Q of errors per canopy density class.....	24
Figure 3-6: UAV and field point derived CHM for block 1.....	25
Figure 3-7: UAV and field point derived CHM for block 2.....	26
Figure 3-8: Digitized tree crown in block 1 and 2 .....	26
Figure 3-9: Tree height estimated from UAV and field data for block 1.....	27
Figure 3-10: Tree height estimated from UAV and field data for block 2.....	27
Figure 3-11: Model development result from each canopy density class.....	29
Figure 3-12: Linear regression through the origin between predicted and measured DBH per canopy density class.....	30
Figure 3-13: Block 1 aboveground carbon estimated from UAV and field data. ....	31
Figure 3-14: Block 2 aboveground carbon estimated from UAV and field data. ....	31
Figure 4-1: Relation between skewness, mean, mode, and median .....	33
Figure 4-2: Field point and UAV DTM.....	34
Figure 4-3: Points in block 1 canopy density.....	36
Figure 4-4: Points in block 2 canopy density.....	36

## LIST OF TABLES

---

Table 2-1: List and use of field equipment.....	7
Table 2-2: List of software used.....	7
Table 2-3: Canopy density class .....	9
Table 2-4: Parameters used for UAV image acquisition.....	10
Table 3-1: Summary of descriptive statistics of measured DBH.....	21
Table 3-2: Result of Shapiro significance test.....	21
Table 3-3: UAV image processing information.....	23
Table 3-4: UAV DTM accuracy assessment.....	23
Table 3-5: F-Test Two-Sample for Variances.....	24
Table 3-6: t-Test result.....	25
Table 3-7: Average tree height per canopy density class.....	28
Table 3-8: F test for tree height per canopy density.....	28
Table 3-9: F-Test Two-Sample for Variances.....	32
Table 3-10: Aboveground carbon t-Test result.....	32
Table 4-1: Mean and median per canopy density class .....	33
Table 4-2: Points statistics per canopy density class.....	35
Table 4-3: Ground points percentage decrease.....	35

## LIST OF EQUATIONS

---

Equation 1a: Error in elevation.....	17
Equation 1b: Mean error.....	17
Equation 1c: Root mean square error.....	17
Equation 1d: Standard deviation.....	18
Equation 2: Normalized mean absolute deviation.....	18
Equation 3a, 3b: Canopy height model.....	19
Equation 4a, 4b: Allometric equations.....	20

# LIST OF APPENDICES

---

Appendix 1: Field data collection sheet.....45  
Appendix 2: DBH-CPA models .....46  
Appendix 3: Python code.....48

## LIST OF ACRONYMS

---

2D	Two-Dimension
3D	Three Dimension
AGB	Aboveground biomass
AGC	Aboveground carbon
CHM	Canopy Height Model
CO <sub>2</sub>	Carbon dioxide
CPA	Crown Projection Area
DBH	Diameter at Breast Height
DTM	Digital Terrain Model
DSM	Digital Surface Model
GCP	Ground Control Point
GNSS	Global Navigational Satellite System
IDW	Inverse Distance Weight
IMU	Inertia Measurement Unit
IPCC	Intergovernmental Panel on Climate Change
LAS	Log Ascii Standard
LiDAR	Light Detection and Ranging
ME	Mean Error
MRV	Monitoring, Reporting, Valuation
NMAD	Normalized Mean Absolute Deviation
OBIA	Object-Based Image Analysis
PPM	Part Per Million
PPP	Public Private Partnership
RADAR	Radio Detection and Ranging
REDD+	Reducing Emission from Deforestation and Forest Degradation
RGB	Red Blue Green
RTK	Real Time Kinematics
RMSE	Root Mean Square Error
SD	Standard Deviation
SfM	Structure from Motion
TIN	Triangulated Irregular Network
UAV	Unmanned Aerial Vehicle
UNFCCC	United Nation Framework Convention on Climate Change



# 1. INTRODUCTION

## 1.1. Background

Global warming is caused by the rise in the concentration of greenhouse gases (such as carbon dioxide) in the atmosphere, resulting in trapping longwave radiation (Grace et al., 2014). Global warming has many undesirable effects such as temperature and sea level rise, more extended drought, precipitation change, and hurricanes (NASA, 2018). The increase in greenhouse gases is mostly due to human activities such as deforestation, forest degradation, industrialization, land use and land cover changes (Baccini et al., 2012; Malhi, 2010).

Forests are vital in mitigating global warming as it absorbs a large part of carbon dioxide (CO<sub>2</sub>) emitted into the atmosphere through photosynthesis (Gibbs et al., 2007). About 31% of total land on Earth is forest which stores more carbon dioxide than any other ecosystem (Saatchi et al., 2011). Although forest stores CO<sub>2</sub>, degradation and destruction of forest releases an enormous amount of CO<sub>2</sub> into the atmosphere, hence increasing the volume of greenhouse gases (Mohren et al., 2012). According to the 2013 report on climate change by the Intergovernmental Panel on Climate Change (IPCC), about 10% of net global emission is due to the conversion of forest land to other land use (IPCC, 2013).

Among the different forest types, the tropical forest has the most substantial CO<sub>2</sub> sequestration rate (Mohren et al., 2012). However, the frightening rate of tropical forest degradation and deforestation has made CO<sub>2</sub> the highest anthropogenic contributor to greenhouse gases, next to only fossil fuels (Hirata et al., 2009). To reduce the emission of greenhouse gases, United Nation Framework Convention on Climate Change (UNFCCC) was established and is based on monitoring and reporting the status of forest carbon (Peltoniemi et al., 2006).

The United Nation Framework Convention on Climate Change (UNFCCC) introduced the Reducing Emission from Deforestation and Forest Degradation (REDD+) program to mitigate global warming through forest carbon sequestration (Scheidt & Work, 2018). The REDD+ program was initiated to protect the forest by reducing forest degradation and deforestation among member countries (Graham et al., 2017). The participating countries report annually on their CO<sub>2</sub> emission and sequestration through the Monitoring, Reporting, and Verification (MRV) mechanism (UNFCCC, 2018). Introduction of the REDD+ programme has led to scientific research for methods to assess the compliance of participating countries to the REDD+ program (Castedo-Dorado et al., 2012).

The MRV of forest carbon stock requires methods that are affordable and give accurate estimates of forest biomass (Kauranne et al., 2017). Forest biomass is the plant-produced organic materials above the soil (such as stalk, seeds, leaves) and roots (Hussin, 2018). Forest biomass includes both below and above-ground forest biomass; however aboveground forest biomass accounts for about 70% to 90% of total forest biomass (Cairns et al., 1997). Forest aboveground biomass estimation is crucial in aboveground carbon stock mapping as aboveground carbon is about 47-50% of forest aboveground biomass (Zaki et al., 2016). Aboveground carbon can give indications of the carbon sequestration rate, the forest carbon stock, and the possible carbon emitted into the atmosphere during forest fire, deforestation or forest degradation (Blanc et al., 2009). Hence there is a need to estimate aboveground carbon accurately.

Aboveground carbon can be accurately estimated using the harvesting method which involves felling, drying and weighing all parts of a tree but the method leads to forest degradation, deforestation, and release of carbon (Basuki et al., 2009). In addition, the process is expensive in terms of labor, time, cost and covers a small area (Hussin, 2018). Although the harvesting method has many disadvantages, it is required to develop an allometric equation that can be used to estimate subsequent forest biomass using non-destructive methods (Yuen et al., 2016). Input for allometric equations can include diameter at breast height, tree height, crown projection area, and tree species (Basuki et al., 2009). Estimating forest aboveground biomass through the non-destructive method requires accurate measurement or estimates of forest parameters and using an appropriate allometric equation (Kankare et al., 2013). The non-destructive method includes field measurement and remote sensing methods. Field measurement is

expensive (cost, time, and energy) and covers a small area while remote sensing provides a cost-effective means of measuring forest parameters over large and inaccessible areas (Böttcher et al., 2009). Moreover, remote sensing data can be used to develop a systematic observation for monitoring and evaluating past and present carbon stock which can be used to project future carbon stock changes thereby explaining the carbon stock dynamics of the area.

Optical remote sensing data can be used to map aboveground carbon, but the spatial resolution significantly affects the accuracy of aboveground carbon estimated. With a medium or coarse resolution (5m or higher) optical remote sensing data, it might be difficult to identify individual trees depending on the size, spacing and crown projection of the tree. The estimated aboveground carbon from medium or coarse optical satellite image can be influenced by soil, grass, or any other feature if the pixel that contains the tree also entails these features. To be able to map accurately aboveground carbon, it is necessary to extract individual trees from the background (soil, branches, or weed) to reduce or eliminate the background influence on aboveground carbon estimated. Boisvenue et al. (2016) compared aboveground carbon estimated from field measurements and optical remote sensing. The results from the studies indicated that medium resolution optical remote sensing data could not be accurately used to estimate aboveground carbon. The availability of high-resolution (below 5m) optical satellite data has shown more promise in mapping aboveground carbon with satellite imagery as it entails enough details to identify individual trees. Baral (2011) estimated aboveground carbon from high-resolution satellite imagery (1 m) and concluded that high-resolution satellite imagery could be used to estimate aboveground carbon. However, the disadvantages are that cloud and shadow which affect optical remote sensing data can lead to data occlusion (Rodríguez-Veiga et al., 2017). Also, the optical satellite images can only provide two-dimensional (2D) but not three-dimensional (3D) forest parameter such as tree height.

Light Detection and Ranging (LiDAR) data are remotely sensed data that can be used to extract 3D forest parameters (Jung et al., 2011). Research has shown that LiDAR data can be used to acquire forest parameters that can be used to estimate forest aboveground biomass and carbon with high accuracy (Brovkina et al., 2017; Ene et al., 2016; Ferraz et al., 2016; Hyypä et al., 2012). However, LiDAR data can be expensive for regular forest monitoring and is not readily available everywhere (Pirotti, 2011).

Unmanned Aerial Vehicles (UAV's) are relatively new devices that can be used to acquire high spatial and temporal resolution imagery (Turner et al., 2012). The UAV image acquisition can be planned to suit the intended purpose while reducing the effect of weather on the image quality which is vital in reaching the REDD+ MRV goals (Getzin et al., 2012). Unmanned Aerial Vehicle (UAV) can also be used to supplement field-based forest inventory measurement as it can be used to acquire images at any time of the day provided illumination and weather conditions are good (Messinger et al., 2016).

There are three main types of UAV namely: fixed wing, rotor based, and a hybrid version (combination of fixed wing and rotor functionality) (Chapman, 2019). Unmanned Aerial Vehicle's (UAV) can carry different cameras such as red-green-blue (RGB) camera, multispectral camera (such as Sequoia), and even LiDAR sensor but this usually depends on the weight of the UAV and the camera (PrecisionHawk, 2018). Unmanned Aerial Vehicle (UAV) was used mainly for military purposes until recently where many civil applications (such as forestry and agriculture) also employ UAV's (Shahbazi, Théau, & Ménard, 2014).

The emergence of UAV coupled with the advance in computer vision and photogrammetry has made it possible to obtain 3D information from 2D images at a relatively low cost. Sensors onboard the UAV are used to obtain cloud-free, high temporal, and spatial resolution images (Tomašítík et al., 2017) which are processed using Structure from Motion (SfM) technique to obtain 3D information (MathWorks, 2018). Structure from motion is a photogrammetric method of acquiring 3D information from overlapping 2D images through stereo vision (Nex, 2018b). For the structure from motion technique to work, images with overlaps captured at different location



(Figure 1-1) are used to identify similar features (tie point) in the overlapping images.

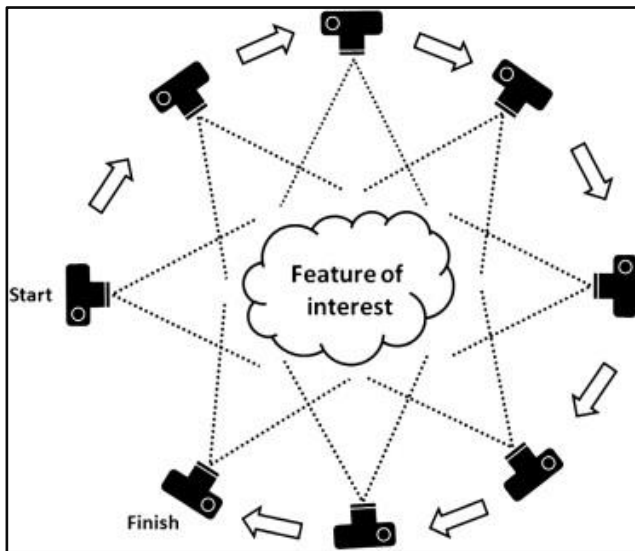


Figure 1-1: A series of overlapping photographs as input for structure from motion (Westoby et al., 2012).

These tie points are identified and traced from one image to the other and used to estimate the initial camera position and coordinates of features (point clouds). From the tie points, the camera position and geometry of the scene (image block) are automatically reconstructed (Westoby et al., 2012). The initial solution is then iteratively enhanced using least-squares minimization (Snavely et al., 2008). The camera position and point clouds derived from the structure from motion method are relative because it is not referenced to real-world coordinates, has no scale and orientation which can be provided by ground coordinates. The generated point clouds which are in a “relative image space coordinate system” are then georeferenced to a “real world object space coordinate system” with the aid of ground control points (Westoby et al., 2012).

The generated points are classified into the ground and non-ground points. The ground points are interpolated to obtain a Digital Terrain Model (DTM) while all the points are interpolated to get a Digital Surface Model (DSM). Orthophotos are then generated from the DSM and image block through the orthorectification process (Nex, 2018a). The orthorectification process is the process of removing the effect of tilt and relief from an image to produce a constant scale planimetric image (Esri, 2016b).

The DTM, DSM, and orthophoto obtained from UAV data can be used to estimate forest parameters (DBH, tree height, and species). Crown projection area (CPA) can be derived from the orthophoto and research has proved that there exists a relation between field-measured DBH and the crown projection area (Hirata et al., 2009; Shimano, 1997). This implies that from the crown projection area, DBH can be estimated. The arithmetic difference between the DSM and DTM can be used to obtain the canopy height model (Lisein et al., 2013). With the crown projection area (CPA) and canopy height model, the tree height can be estimated. With these parameters (DBH and tree height), an appropriate allometric equation and a conversion factor can be used to estimate aboveground carbon.

## 1.2. Research problem

The relatively low cost and usefulness of UAV have caused a global rise in the use of UAV for surveying. However, the quality of the result obtained from processing UAV images should be assessed.

Berhe (2018) and Odia (2018) used UAV acquired images to extract forest parameters (such as crown projection area and tree height). These parameters were input in an allometric equation to estimate aboveground carbon. The result from the research indicated that the accuracy of aboveground carbon estimated depends on the accurate estimation of the crown projection area and tree height.

Object-Base Image Analysis (OBIA), a remote sensing processing method that does not use only spectral information but also textural and geometric properties to detect features can be used to generate crown projection area with reasonable accuracy depending on the image resolution and canopy layers (Gomes & Maillard, 2016). However, tree height which is estimated from the Digital Surface Model and Digital Terrain Model can be inaccurate especially in a dense forest.

Unlike Radio Detection and Ranging (RADAR), UAV sensors cannot penetrate canopy cover making it very difficult for UAV to image the forest floor especially in a dense canopy forest (Wallace et al., 2016). If the forest floor is difficult to image, then less tie points and subsequently few points will be generated on the forest floor in contrast to the top of the canopy where more tie points will be generated. The generated points are used to create the Digital Terrain Model (DTM) and Digital Surface Model (DSM) but the quality of the DTM and DSM depends on the quality, quantity, and distribution of points used (Nex, 2018a). Due to this, the quality of DTM generated in a dense forest will be poor compared to the generated DSM where more points are generated on the forest canopy. With an accurate DSM but a less accurate DTM, the tree height estimated may not be representative of the actual tree height and may result in inaccurate estimation of aboveground carbon (Ota et al., 2015).

To improve the estimation of tree height, some researchers proposed using the mean of the pixels per crown projection area (Ota et al., 2015; Ioki et al., 2014). However, Ota et al., (2015) in their research concluded: “to accurately estimate AGB, we need a more accurate DTM than the DTM derived from aerial photographs using the Structure from Motion approach.”

Although research has been carried out in accessing the quality of Digital Terrain Model and its effect on the estimation on canopy height model, no study has been found that considered the influence of canopy density on the estimation of UAV generated DTM as different forest canopy density will have different effect on point generated and subsequently DTM created.

The canopy density of the forest depends on the forest type. Plantation forest has trees planted at regular interval hence reducing the effect of intermingling crown and canopy layer. Also, the canopy density of the plantation depends on the age of the plantation forest. Unlike plantation forests, natural and riparian forests have different tree species at irregular spacing hence increasing the crown intermingling effect and making the canopy denser. Also, the different tree species have different growth and development. Hence the tree layers will be different which also makes the forest canopy denser and difficult for the UAV to image the forest floor. All these affect the quality of the Digital Terrain Model generated from UAV. Hence, the main aim of this study is to assess the accuracy of UAV-DTM generated under different forest canopy density (open, medium and dense) and its effect on the estimation of aboveground carbon.

### **1.3. Research objectives**

The primary objective of this research is to assess the quality of UAV-DTM generated under different canopy density and its effect on the estimation of aboveground carbon.

The specific objectives are:

- a) To assess the accuracy of DTM generated from UAV images under different forest canopies.
- b) To model the relation between CPA and field measured DBH.
- c) To model tree height from field point and UAV data.
- d) To evaluate the effect of different canopy density on the estimation of aboveground carbon.

### **1.4. Research questions**

- a) What is the accuracy of UAV-DTM compared to field points under different forest canopy density?
- b) What is the relation between CPA and field measured DBH?
- c) What is the difference in tree height generated from UAV-CHM and field-CHM?
- d) What is the difference in the aboveground carbon estimated from UAV dataset compared to field point?

### 1.5. Research hypothesis

- a) H0: There is no relation between root mean square error and canopy density.  
H1: There is a relation between root mean square error and canopy density.
- b) H0: There is no relationship between CPA and field measured DBH.  
H1: There is a relationship between CPA and field measured DBH.
- c) H0: There is no significant relationship between UAV-CHM and field CHM.  
H1: There is a significant relationship between UAV-CHM and field CHM.
- d) H0: There is no significant difference in aboveground carbon estimated from UAV and field data.  
H1: There is a significant difference in aboveground carbon estimated from UAV and field data.

### 1.6. Conceptual diagram

The system boundary for this research is Asubima forest in Ghana. The input to this system is the sun which emits rays. The emitted sun rays interact with the atmosphere. Some of the emitted sun rays are absorbed and reflected by the atmosphere, while others are transmitted. The transmitted sun rays reach the system (forest) and interact with the trees in the forest system.

The trees also interact with the atmosphere by absorbing carbon dioxide and releasing oxygen during the day. At night, the trees release a small amount of carbon dioxide. The interaction between the sun rays, atmosphere and trees in forest results in changes to tree height and DBH through photosynthesis.

The UAV interacts with the sun rays which interact with the trees. From this interaction, the amount of aboveground carbon stored in the trees can be estimated. The conceptual diagram below (Figure 1-2) shows the various systems and interactions within the system.

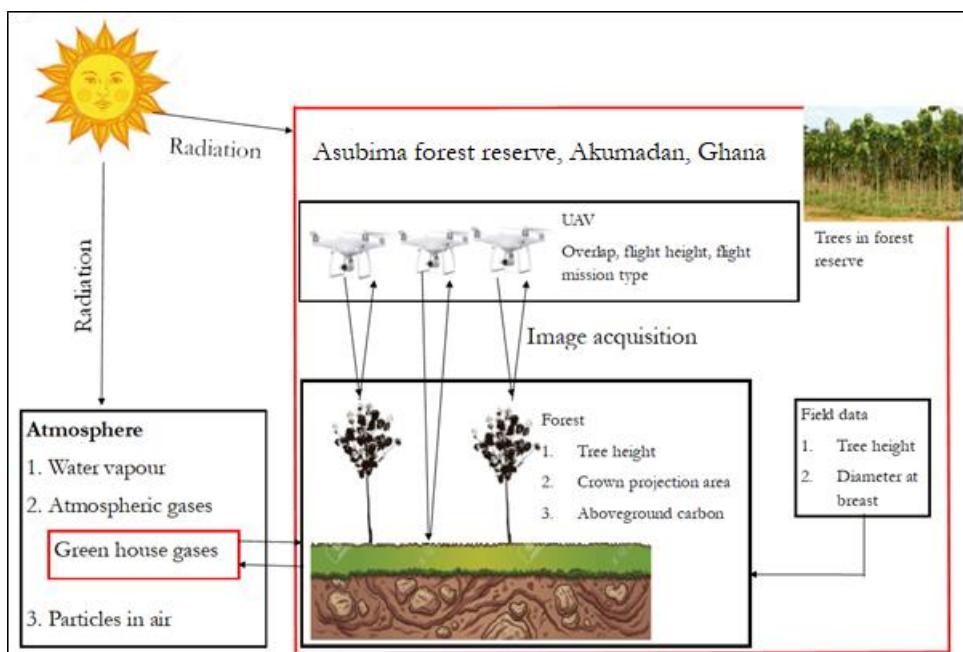


Figure 1-2: Conceptual diagram of system interactions

The UAV used in this study has only RGB camera on-board, hence can only receive rays from the sun in the visible wavelength range. The visible rays cannot penetrate the canopy but hit the top of the tree canopy and is reflected. In an open space, the sun rays hit the ground and reflected. The sensor on the UAV receives the reflected rays. The research mainly uses the interactions between the UAV and forest canopy to investigate the accuracy of UAV-DTM and its effect on estimating aboveground carbon.

## 2. STUDY AREA, MATERIALS, AND METHOD

### 2.1. Study area

The research was carried out in Asubima forest which is a degraded forest in the Ashanti region of Ghana and under the authority of Offinso District Forestry Commission. The geographical location of the reserve is between 621700m E – 628000m E and 812800m N – 822600m N. The forest is about 100 km from Kumasi (Ashanti regional capital) and shown in Figure 2-1 below.

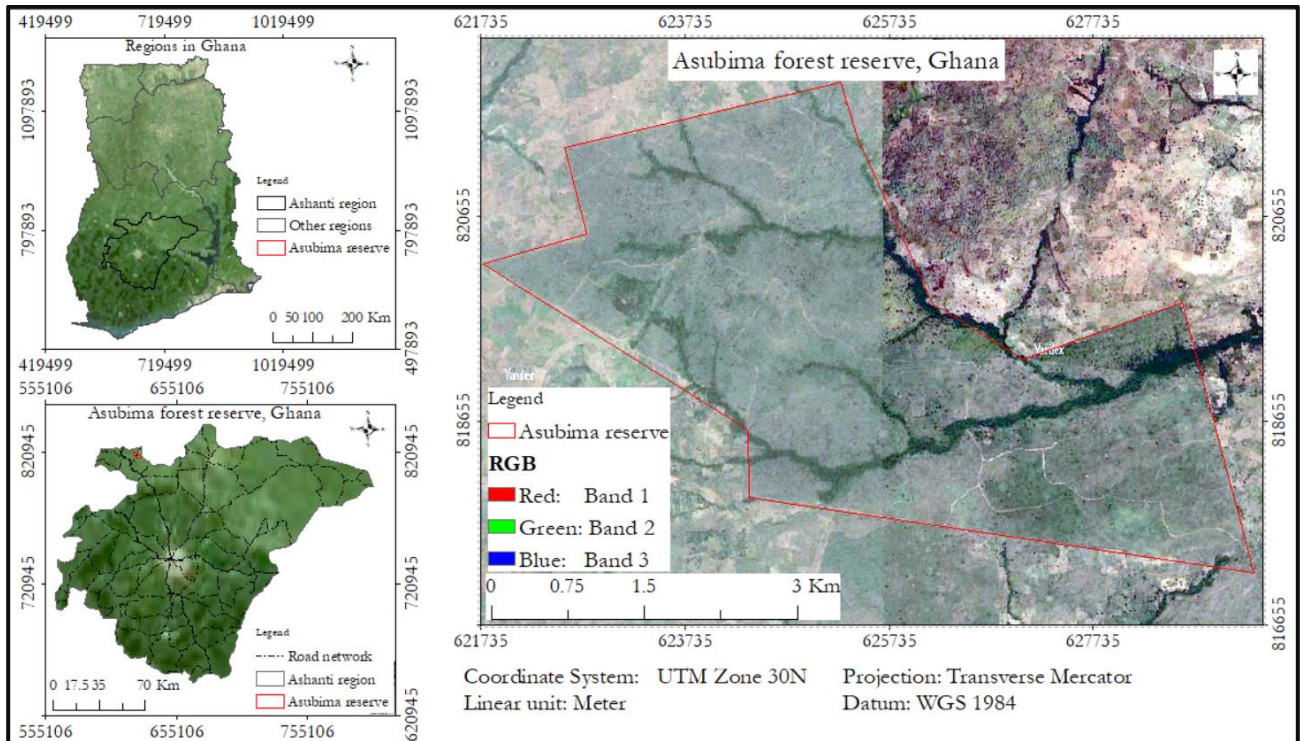


Figure 2-1: Map of Asubima forest reserve, Ghana.

The forest was hugely degraded due to activities such as forest fire, illegal farming and logging. In an attempt to reforest the area which lies in the dry semi-deciduous ecological zone, a private forestry company (FORM Ghana) was given about 3,500 ha out of 11,130 ha for teak plantation through the Public Private Partnership (PPP) agreement (Wanders, 2017). The PPP agreement was between the Forestry Commission of Ghana, traditional landowners, and Form Ghana with the aim of restoring the degraded forest through the establishment of forest plantation (World Bank, 2016).

#### 2.1.1. Climate

There are two main climate seasons namely the wet (rainy) and dry seasons. The dry season generally begins from November to March and July to August while the wet season begins from March to July and September to October. The area has an annual average temperature and rainfall of 26°C and 1227 mm respectively with the warmest months between February and March (Wanders & Tollenaar, 2017).

#### 2.1.2. Vegetation

The composition of tree species in the study area is about 90% of *Tectona grandis* (teak) and about 10% of mixed indigenous species such as *Triplochiton scleroxylon* (Wawa), *Milicia excelsa* (Odum), and *Entandrophragma cylindricum* (Sapele). The natural and riparian forest were conserved.

Enrichment planting was carried out in the riparian forest to improve the riparian forest which enhances biodiversity, reduce erosion, and protects the water from erosion. The riparian forest also serves as habitat for wildlife and controls pollution of the stream.

## 2.2. Material

Different field equipment, as shown in Table 2-1 below, were used to acquire the data needed for this study.

Table 2-1: List and use of field equipment

I.D	Purpose	Field instrument
1	Taking pictures of forest canopy density	Canon EOS 60D camera with fisheye lens
2	To measure 3D ground data	Trimble R10 RTK system with external radio and elevated external antenna for base
3	To mount base of Trimble R10 equipment	Tripod
4	External power supply	Boliden car battery
5	For UAV survey	DJI Phantom 4 Pro
6	To establish temporary GCP	GCP plastic target
7	To measure the height of trees	Suunto clinometer
8	To measure the diameter of trees	Diameter tape
9	To measure base to aid tree height measurement	Measuring tape
10	Record measurement on field	Data recording sheet
11	UAV flight planning and navigation	iPhone 6S
12	For making way in the forest	Cutlass

In this study, Real Time Kinematics (RTK) survey points (field points), biometric data (DBH and tree height), hemispherical and UAV images were collected from the field and used for analysis. As the study aims to evaluate the error in UAV DTM, it was imperative to measure the elevation of the terrain as accurate as possible to serve as reference data. Hence the RTK survey was used because it can measure 3D coordinates at sub-meter accuracy and takes less time (Trimble, 2014). Data collection was between 20<sup>th</sup> September to 17<sup>th</sup> October 2018.

Different software was used to acquire and process the data to obtain the required result. Table 2-2 below shows a list of software used.

Table 2-2: List of software used

I.D	Purpose	Software
1	Spatial analysis, map making, and digitizing	Arc Map 10.6.1
2	Processing images from the hemispherical camera	Gap Light Analyzer 2.0
3	Processing UAV acquired images	Agisoft Photoscan Professional 1.4.3
4	Thesis writing	Microsoft Word 2016
5	Thesis presentation	Microsoft PowerPoint 2016
6	UAV flight planning	Pix4D capture
7	UAV setting and configuration	DJI 4 Go
8	Flowchart	yED Graph Editor
9	Statistical analysis	Microsoft Excel 2016, R
11	Referencing and citation	Mendeley Desktop
12	Extracting coordinates	Google Earth Pro
13	Point cloud analysis	LAStools
14	Geoatabase for research	Arc Catalogue 10.6.1
15	Filtering UAV tie point	Python

## 2.3. Method

The method used in the study can be grouped into three (3) parts.

Part 1 was reconnaissance survey and data collection which involved topographic survey, biometric data collection,

hemispherical and UAV images capture.

Part 2 was data processing which involved processing the data obtained in Part 1 to obtain Digital Surface Model, Digital Terrain Model, and orthophoto. The tree crowns were also digitized and canopy height model developed from both UAV and field point data.

Part 3 was data analysis which involved analysing the result obtained from Part 2 to answer the research questions. From the analysis, the accuracy of the UAV DTM was assessed by calculating the root mean square error per canopy density class to answer research question 1. Also, the relation between the CPA and its associated DBH was determined to answer research question 2. Furthermore, the difference or similarity between tree height estimated from UAV and field data was determined to answer research question 3. Finally, aboveground carbon was estimated from UAV and field point data per canopy density class. The influence of the canopy density was determined by evaluating if the difference in aboveground carbon estimated from UAV and field point data was significant to answer research question 4.

Figure 2-2 below shows a flowchart of the method.

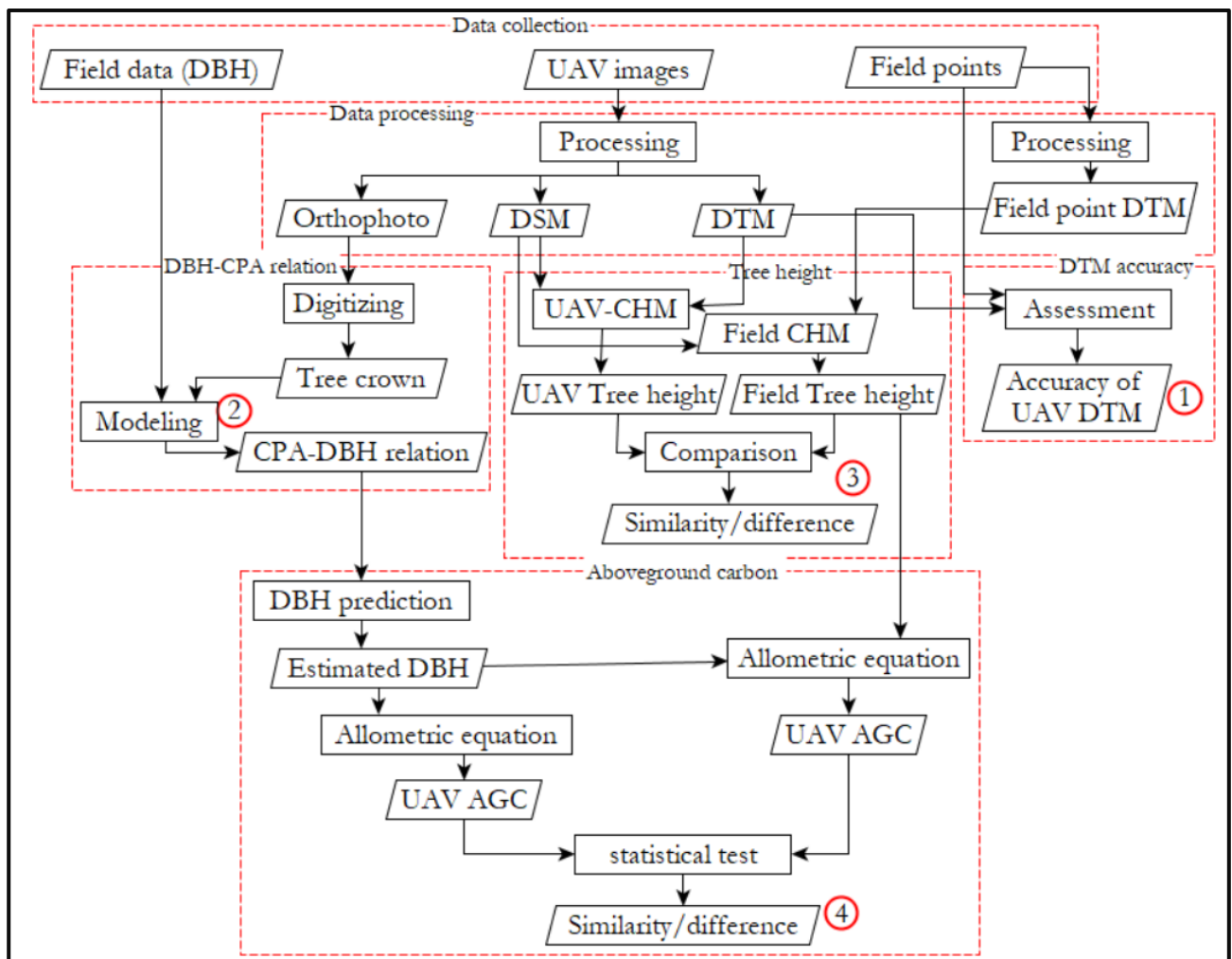


Figure 2-2: Flowchart of the implemented method

## 2.4. Pre-fieldwork

Before the fieldwork, an overview of the canopy density classes to be used for the survey was determined by downloading Google Earth images and observing the variation in canopy density. From the Google Earth images, two main canopy density classes (plantation and riparian forest) were identified.

The Google Earth images were also used to identify open spots where plastic ground control points (GCP) could be placed. Furthermore, the images were used to design the optimal locations to set the temporal benchmark to be used for the topographic survey.

## 2.5. Fieldwork

### 2.5.1. Reconnaissance and canopy density image capture

The first activity performed during the fieldwork was reconnaissance survey to verify where the canopy density classes are located and also check for accessibility as the fieldwork was carried out in the raining season.

During the reconnaissance survey, Canon EOS 60D camera with fisheye lens was used to take images of the forest canopy. The hemispherical images were processed using Gap Light Analyzer to obtain the forest canopy density. The calculated canopy density was then classified using the Forest survey of India classification reference and the threshold shown in Table 2-3 below.

Table 2-3: Canopy density class (source: Forest survey of India)

Forest canopy class	Canopy cover range (%)
Open forest	10 - 40
Medium forest	40 - 70
Dense forest (teak and riparian)	70 and above

Based on the canopy density classification (Table 2-3), four canopy density classes were identified namely: open canopy, medium canopy, dense canopy (plantation), and dense canopy (riparian forest). Open and medium canopy density were in a teak plantation. The dense canopy comprised a dense teak plantation and dense riparian forest. These canopy density classes were stratified to analyze and estimate its effect on the quality of DTM generated by UAV.

Two blocks of about 5 hectares were identified to be used for the UAV flight. Within the blocks for the UAV flight, the canopy density classes are located. Canopy density class of about 0.5 hectares was established and the DBH and height of a number of randomly selected trees measured. The trees in the plantation forest were planted at an interval of 3m by 3m resulting in about 1100 trees in 1 hectare (650 trees in 0.5 hectares). Hence measuring the DBH and height of all the trees in each class was not possible considering the fieldwork duration.

### 2.5.2. Sampling design

Purposively sampling design was used to select the location of the canopy density classes during data collection because the fieldwork was carried out in the rainy season. When it rains, some part of the forest is not accessible due to flooding and bad condition of roads. To efficiently utilize the limited fieldwork time, a purposive sample design was used.

### 2.5.3. UAV mission planning and image acquisition

The UAV data acquisition was carried out using DJI Phantom 4 Pro with RGB camera. After identifying the canopy density classes on the field, the UAV block was selected. The UAV blocks which contains the canopy density class was then selected in such a way that at least two forest canopy density class were present in each UAV block to reduce movement during data acquisition. Figure 2-3 below shows the location of the UAV blocks.

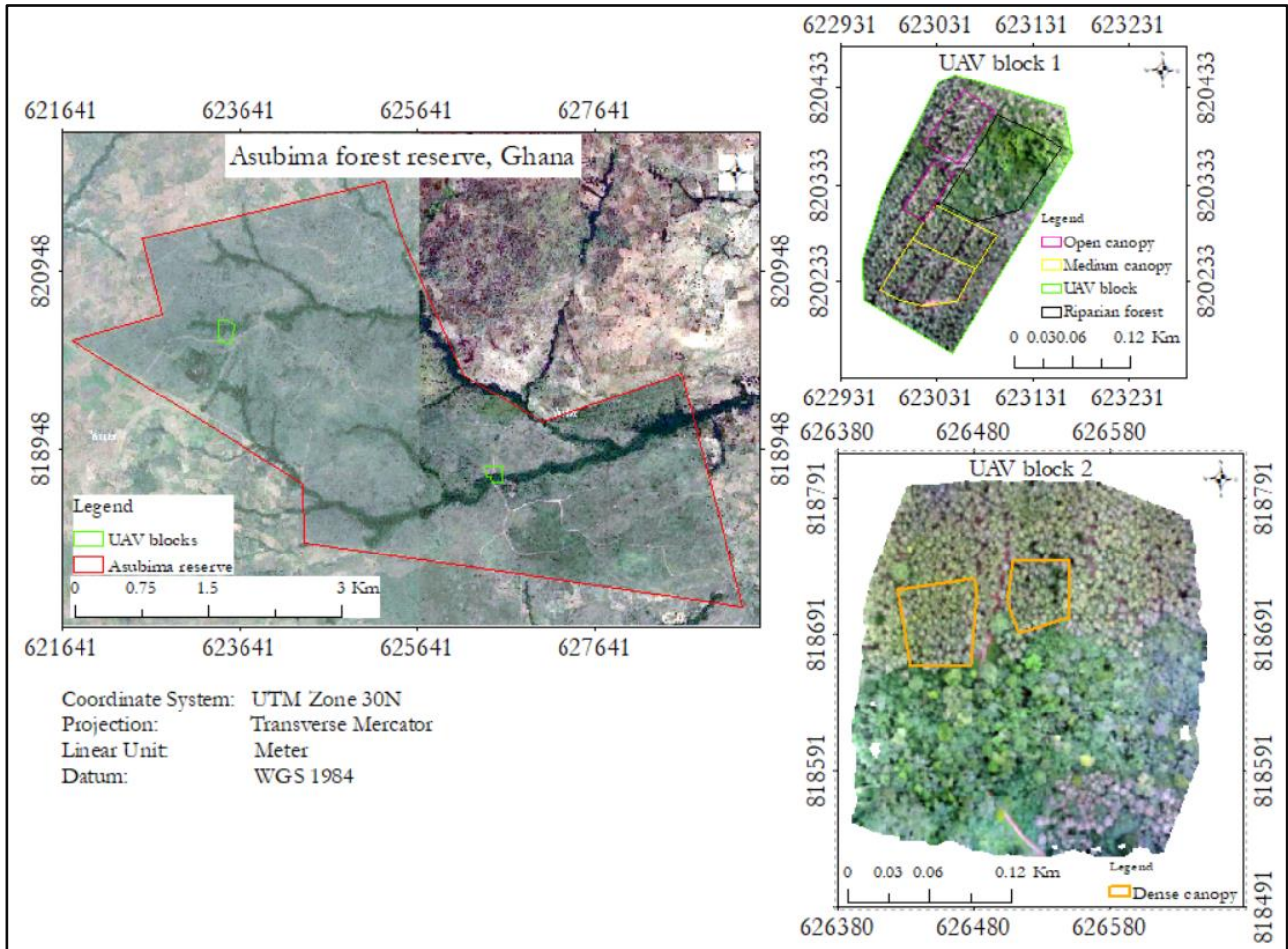


Figure 2-3: UAV blocks in the study area

Before the image acquisition, the UAV compass was calibrated for safety purposes using the DJI Go 4 while the Pix4D capture was used to design the flight plan. The main aim of the research was to assess the quality of DTM generated by UAV which is based on the points generated. To generate dense points, the acquired images must have high overlaps (Pix4D, 2018a; Dandois et al., 2015). Hence flight parameters that ensured the generation of dense points were used as shown in Table 2-4 below.

Table 2-4: Parameters used for UAV image acquisition

Parameter	Flight type	Camera angle	Speed	Altitude	Forward overlap	Side overlap
Input	Double grid	90°	Moderate	60 m	90°	80°

With the GCP fixed at an appropriate location and flight planned, the next step was to acquire the images using the DJI Phantom 4 Pro. Before the flight, we ensured the battery level and connection of the radio and GPS was good. We then flew the two blocks with the same flight plan. However, multiple batteries were used during the flight as the flight time exceeded the battery capacity which is about 30 minutes.

After each flight, the acquired images stored on the memory card of the UAV was transferred onto a laptop and the quality of images assessed using Agisoft Photoscan Professional before going to the next site.

#### 2.5.4. Topographic survey

Digital Terrain Model generally refers to the elevation of the bare ground as a raster grid (Fras et al., 2016). To develop a DTM, 3D points are first measured/deduced and interpolated. To obtain a good DTM, 3D points with elevation representative of the terrain should be used. Measuring such 3D points requires using instruments with acceptable accuracy although the accuracy requirements depend on the use of the DTM (Fras et al., 2016).



Boundary pillars have been established at the boundary of the forest by the Forestry Commission. However, the coordinates of these boundary pillars were obtained using handheld GPS. The handheld GPS has an error of about 3-10 m which will not be useful for the research. This is because the boundary pillars would be used to georeference the UAV images which will introduce these errors in the UAV results. With wrong UAV results, the subsequent parameters (DBH, tree height, and tree location) will be wrong which will lead to incorrect estimation of aboveground carbon. Also, the boundary pillars will be used as a base station to transfer coordinates to the study area for the topographic survey and this will also introduce errors in the topographic survey.

Because of this, a national benchmark established by the Survey Department of Ghana was used to transfer coordinates to the study area. The national benchmark is located at Offinso Municipal Assembly which is about 65 km from Asubima forest. The Trimble R10 instrument which is a Real-Time Kinematic (RTK) Global Navigational Satellite System (GNSS) instrument with external radio was used for the topographic survey to obtain coordinates of sub-meter accuracy even under dense forest canopy (Trimble, 2014). The external radio was used to extend the broadcast range for the signal to 10 km to make the transfer of the coordinate faster.

GNSS is a navigation system that comprises three main segments namely the space segment, the control segment, and user segment. The space segment consists of all the satellite constellation, the control segment includes all monitoring stations, and the user segment comprises of everyone using the GNSS system (Hexagon Positional System, n.d.). Coordinates obtained from GNSS are subjective to errors such as satellite orbital, clock errors, receiver clock error, noise, multipath, and atmospheric (ionosphere and troposphere) refraction (Hosseinyalamdary, 2018). The most significant contributor to the GNSS error is receiver clock. Also, multipath caused by reflection of GNSS signal resulting in the signals having longer travel time, would influence the accuracy of the coordinates measured (ESA, 2012). The accuracy of coordinates obtained from the GNSS survey is dependent on the errors that will be reduced or eliminated. Most of the errors can be eliminated using differential GPS or RTK survey, better receiver, and proper planning resulting in a sub-meter error (Hosseinyalamdary, 2018; Knippers & Tempfli, 2012).

Although the instrument used gives a sub-meter accuracy, it was necessary to check the systematic error. Systematics errors are reoccurring errors that are constantly reflected in the measurement and are in the same direction (WYDOT, 2008). To identify the systematic error of the instrument, the Trimble R10 instrument was used to pick the location of four (4) points with known coordinates (benchmark) repeatedly (five times per benchmark) and the difference between the known and measured coordinates estimated (Knippers et al., 2013). It was detected that the systematic error was -4 mm in eastern, -6 mm in the north, and 3 cm in elevation. To correct the final coordinates, the same magnitude of error but in the opposite direction was added to the recorded coordinates after the topographic survey.

To begin the survey, the road network from Offinso to Akumadan was extracted from the Google Earth images and used to optimize the suitable location to establish a new control point considering the range of the external radio signal. Since the range of the external radio signal used was 10 km, consecutive point along the road at a maximum distance of about 9.5 km from the location of the point with known coordinates (referred to as benchmark) was identified as shown in Figure 2-4 below.



Figure 2-4: Location of benchmark, consecutive point (B1 – B6) and desired base station location.

During the GNSS survey, the tripod was set and leveled on the benchmark, and a plumb bob used to ensure the tripod is at the center of the benchmark. The base of the Trimble R10 was fixed on the tripod and the bubble centered. The external antenna was also fixed on the base station. The external radio was then connected to the external battery and also fixed on the base. The radio signal receiver was then attached to the range pole of the rover. The exact coordinate of the base station received from the Survey Department of Ghana was then entered as base station location. The positional accuracy was set to 0.1 m meaning the accuracy of the point to be picked will not be more than 10 cm as the instrument rejected all errors greater than 0.1 m until the estimated positional accuracy or better (less than 10 cm) is achieved. Also, measurements from angles less than  $30^{\circ}$  were ignored to reduce multipath error

The height of the base station and rover stand were then measured and entered in the receiver after creating a file on the Trimble R10 rover to save the coordinates and the RTK mode activated for the survey to begin as shown in Figure 2-5 below.

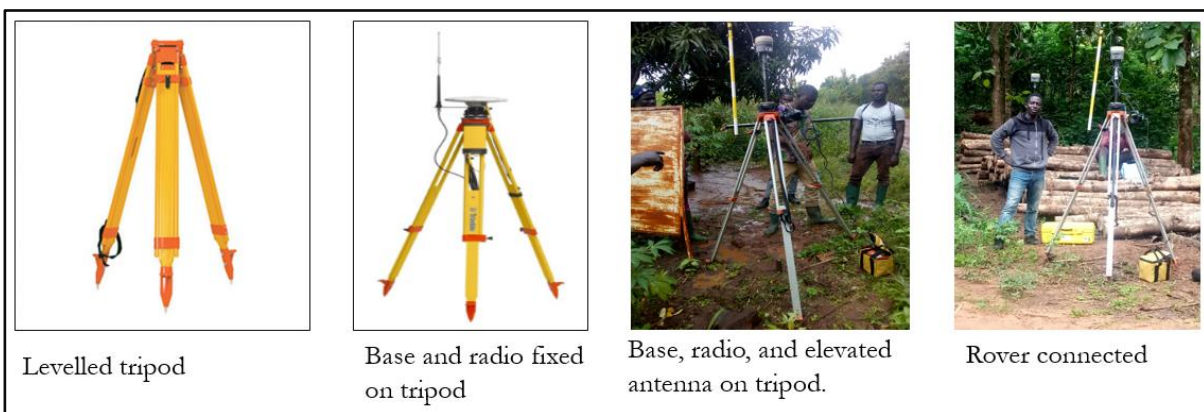


Figure 2-5: Summary of the GNSS setup

After setting up the base station on the benchmark (Figure 2-5) and activating the RTK function on the rover, the rover was sent to B1 (Figure 2-4) to measure and save the coordinate. The base then was moved from the

benchmark location to B1 and setup made again. The rover was then moved to B2 and the coordinates measured and saved. This process was repeated until the coordinates were transferred to the desired location (Figure 2-4) in the plantation forest. A vehicle was used to move equipment from the old base station to a new location. While driving, we ensured that the radio signal was not lost by moving less than 10 Km from the base station.

The main reason for the topographic survey was to generate DTM for the study area with more focus on the canopy density classes. Hence more points (minimum of 60 points per canopy density class) were picked within the canopy density classes while additional points were picked outside the canopy density class to improve the quality of DTM generated at the boundary of the canopy density class. Figure 2-6 below shows the field points per blocks.

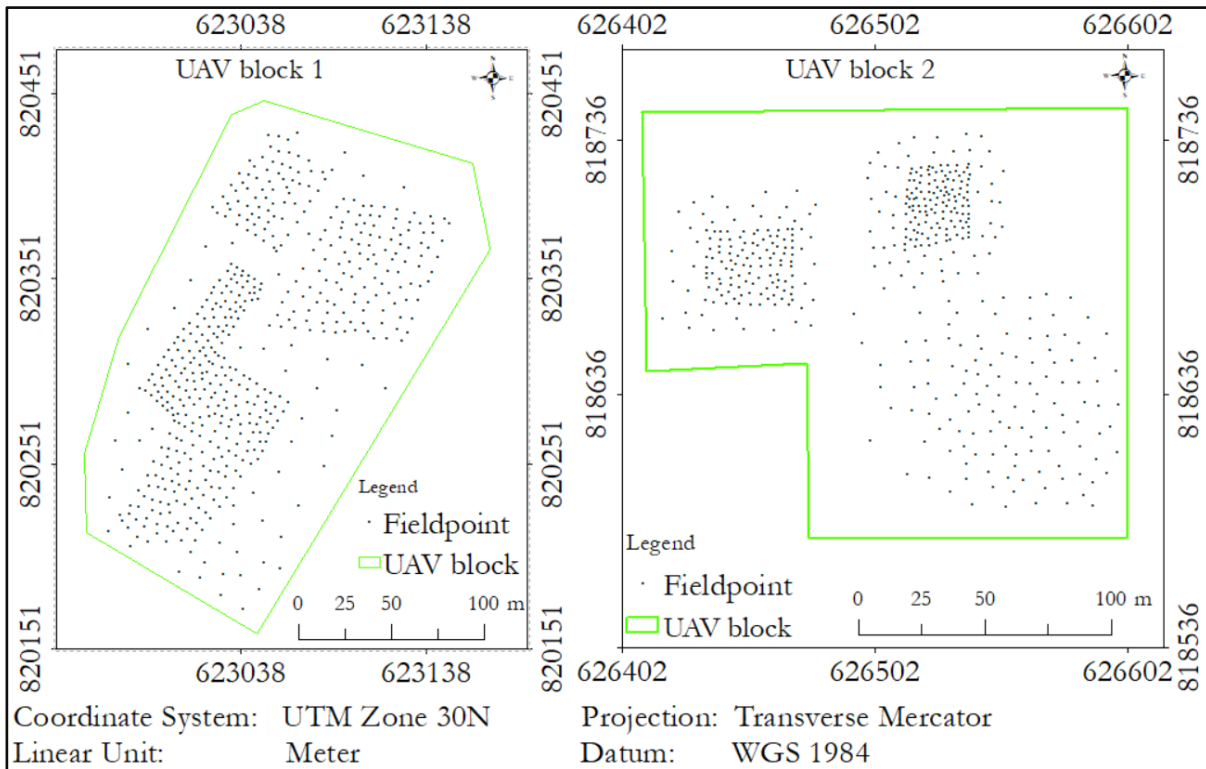


Figure 2-6: Field points within each UAV block

From Figure 2-6 above, block 1 contains more field points compared to block 2 because more canopy density class are located in block 1 compared to block 2. Block 1 contains the medium, open and riparian class while block 2 contains the dense canopy density class (Figure 2-3).

As can be observed from Figures 2-3 and 2-6, the size of block 2 is not consistent. This is because only the section of block 2 that contained the canopy density was used for the RTK survey. Hence after the UAV image processing, only the section of block 2 containing the canopy density classes will be used for further analysis.

### 2.5.5. Biometric data collection

In addition to the above, the DBH and tree height were measured on the field. Before the biometric measurement, the UAV data were processed using Agisoft Photoscan Professional software to obtain the Digital Surface Model (DSM) and orthophoto of each block. The DSM and orthophoto were printed on an A3 paper to be used for identification of individual trees.

To identify individual trees, big trees found in the study area was used for orientation. The planting interval in the plantation forest also aided the easy identification of the teak-trees. After identifying the trees on the orthophoto and the ground, the identified trees were marked on the orthophoto and an ID assigned. The DBH and tree height were measured using diameter tape and clinometer respectively.

Not all trees within each canopy density class could be measured (see 2.1.1), hence there was a need to develop a model that can predict the unmeasured DBH. To develop the model, trees of varying DBH is required to explain the variability in the model (Shimano, 1997). Hence, trees of varying DBH were selected and measured. Dead trees were not measured.

When measuring the DBH, the tape was at the height of about 1.30 meters above ground. The tree height were measured with Suunto clinometer by using a tape measure to measure the ground distance of 15 m or 20 m (depending on the distance where the top and base of the tree are observable) and taking the reading at the top and base of the tree. The difference between the top and base of the tree is the height.

Using clinometer for tree height measurement can introduce some errors in the measured tree height. During the field measurement, error in the horizontal distance results in the wrong measurement of tree height. Also, using wrong angle influences the measured tree height. Moreover, in a forest environment where the tree top sometimes cannot be seen, the measured tree height will be wrongly measured. Luoma et al., (2017) evaluated the precision of tree measurement using clinometer and found that tree height measured with clinometer has a standard deviation of about 0.5 m. Due to all these errors, the measured tree height was not used for further analysis but served as a check for tree height estimated from the UAV and field point data.

## 2.6. Data processing

### 2.6.1. Forest canopy density classification

The hemispherical images were processed using the Gap Light Analyser to calculate the canopy openness. The images were loaded and registered in the software by selecting the region to be used for the analysis. A threshold that represents the canopy openness/closeness was chosen to separate the open sky from forest canopy density as shown in Figure 2-7 below.

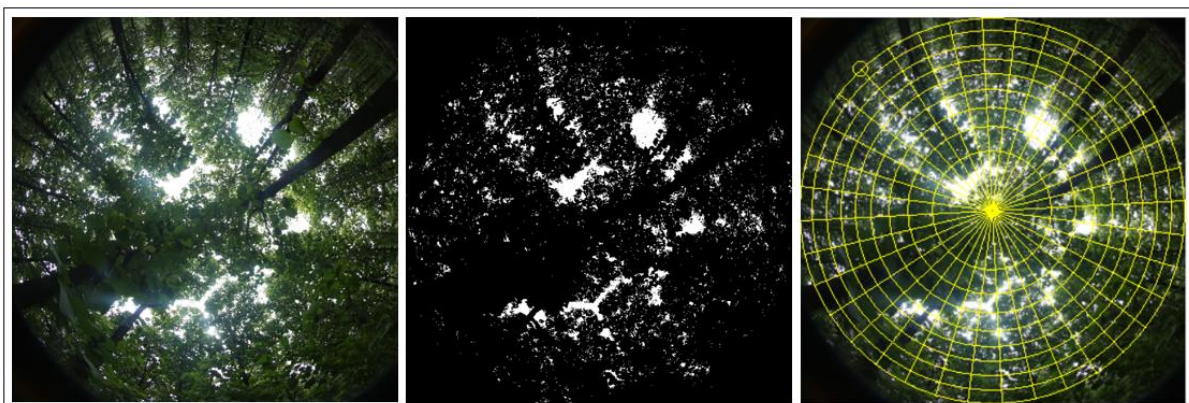


Figure 2-7: Forest canopy density image (left), after applying threshold (middle), and calculating the open area in the image (right).

After separating the forest canopy from the open sky, the canopy cover was calculated and classified using the Forest survey of India classification system (as shown in Table 2-3).

### 2.6.2. UAV image processing

The UAV acquired images were processed using Agisoft Photoscan Professional 1.4.3 software which is based on structure from motion principles. Figure 2-8 below shows the general workflow of UAV image processing.

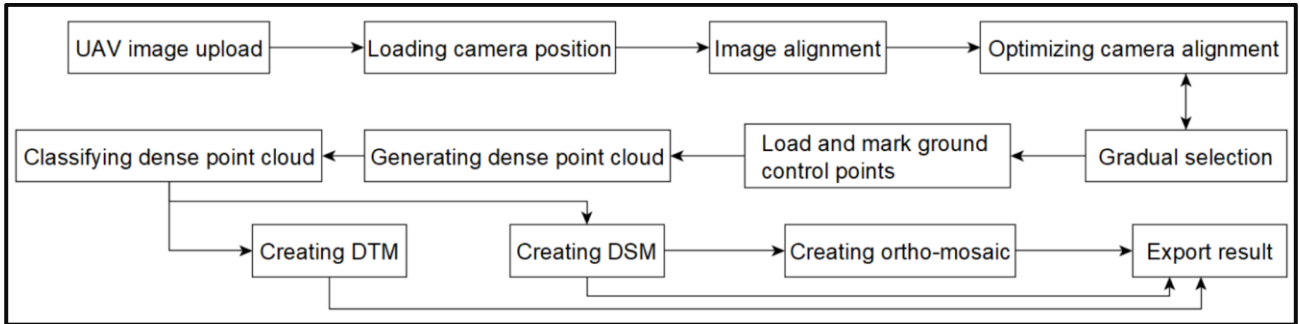


Figure 2-8: Photogrammetric workflow used

Before the UAV image processing, the graphical processing unit (GPU) of the software was activated to enhance the processing speed. The images with its camera position were all loaded in the software. The images captured with the UAV has coordinates because the UAV has GPS receiver and an inertial measurement unit (IMU) on-board however they are low cost and cannot give sub-meter accuracy (Nex, 2018b). The images were used for preliminary georeferencing.

The image alignment, which involves finding similar features on images to reconstruct the camera position from each image was activated to generate tie points (Agisoft, 2018). The tie points are generated by identifying similar features in images. The camera location was also estimated in the image alignment process. The quality of the tie points were assessed by considering the number of image match per tie point. From the assessment, the tie points were found to have weak matches at the edges and this could be because the image overlaps are low at the edges (Pix4D, 2018c). Tie points are essential in generating point clouds. Hence any error in tie points generated will influence the quality of point clouds generated which will affect the quality of DTM and DSM produced (Pix4D, 2018d). Although it is necessary to filter tie point, there is no available function for this in Agisoft Photoscan software. However Agisoft supports python application programming interface (API). Hence a code was developed with Python API to remove weak tie points (shown in Appendix 3).

The camera alignment was then optimized to obtain result of higher accuracy. The camera optimization involves estimating the camera interior and exterior orientations and measurements while correcting for lens distortion through least square bundle block adjustment (Agisoft, 2018).

The gradual selection option was then used to enhance the geometry of the overall model (Agisoft, 2018). Three gradual selection steps were implemented to improve the geometry. Reconstructing uncertainty was the first step implemented. This option eliminates bad points cause by poor geometry after which the camera optimization step was repeated. The projection accuracy step was then implemented to eliminates bad points caused by errors associated with pixel matching. After executing the projection accuracy step, the camera optimization step was repeated. The final step was to eliminate or minimize reprojection error by removing bad points caused by the residual error of a pixel to enhance the accuracy of the tie point. The gradual selection process was implemented to reduce projection and pixel error (Agisoft, 2018).

To further enhance the image processing and to georeference the final output data accurately, the ground control points (GCP) were loaded. The images with GCP were identified and marked as accurately as possible and the corresponding 3D coordinate obtained during the topographic survey entered. The GCP was used to georeference the images. Although the UAV has GPS and inertia measurement unit (IMU) to measure coordinates, the accuracy of the GNSS receiver onboard the UAV is not suitable (in a high precision work) hence the GCP's are used to improve the georeferencing accuracy in order to obtain objects on map whose location on ground is same or almost the same (Nex, 2018a). Out of the 12 GCP's used for the survey, 8 were used as GCP's for georeferencing and the remaining 4 used as checkpoints (CP). The checkpoints are not used in the bundle block adjustment but used in calculating the errors in the image processing by calculating the difference between the control point coordinates and the interpolated surface (Nex, 2018a).

Dense point clouds were then generated and classified to ground and non-ground point clouds. The ground point clouds were then used to generate the Digital Terrain Model while all the point clouds were used to generate the

Digital Surface Model. The Digital Surface Model was used as input to generate the orthophoto. The Digital Terrain Model, Digital Surface Model, and orthophoto were then exported for further analysis.

### 2.6.3. Generating a DTM from field measured points

After the topographic survey in the blocks, the coordinates were exported and the systematic errors corrected. Apart from the systematic error corrections, no other corrections were applied because the errors were corrected in real time when the base station sends the correction to the rover through the radio signal.

All the field (RTK) points were grouped per block and used to generate DTM of the blocks using ArcMap 10.6.1. In generating the DTM, a control experiment was set up to identify the best interpolation algorithm to use. The test was mainly between inverse distance weight (IDW) and triangulated irregular network (TIN) algorithms as these are the algorithms mostly used in UAV processing software (Pix4D, 2018b).

TIN is created from Thiessen polygons which divides a region in such a way that every cell has one value (Tan & Xu, 2014). The Thiessen polygons are based on Delaunay triangulation which requires that the triangles are equilateral and the circumference through its three anchor points does not comprise any other anchor point (Knippers et al., 2013). When the condition for Delaunay triangles are fulfilled, the minimum interior angles of all triangles are maximized resulting in the avoidance of long, thin triangles (Esri, 2016c). The algorithm is used to determine which points are used to form the Delaunay triangle. Because the node can be positioned unevenly over a surface, areas which are undulating can have higher resolution to explain the complexity of the area and vice versa (Esri, 2016c) as shown in Figure 2-9 below.

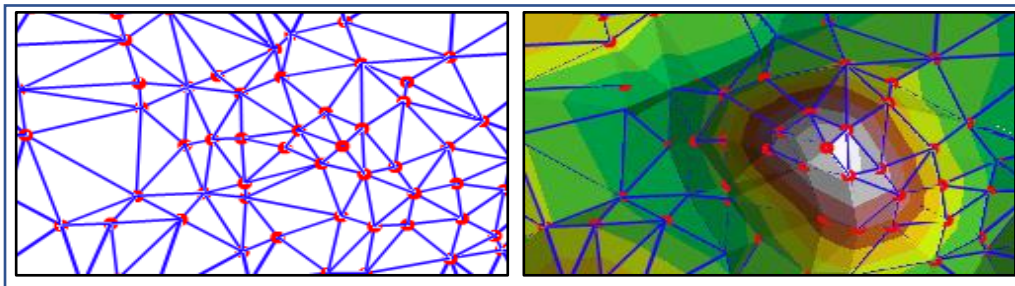


Figure 2-9: Delaunay triangles and the associated DEM (Esri, 2016c).

The location of the input feature used to generate the TIN remains in the same position as the nodes or edges. This enables the TIN to reserve the accuracy and precision of the input data while interpolating the values between the known points (Esri, 2016c).

IDW interpolates the values of an unknown location using a linear combination of values at sampled points by assuming that closer points are more alike than those that are far apart (Li & Heap, 2008). To estimate the values for any location not measured, the measured values around it are used. Based on the assumption of IDW, the known values close to the unmeasured values have more influence on the estimated value than those farther away hence greater weights are assigned to points closest to the prediction location than those farther away (Esri, 2018) as shown in Figure 2-10 below.

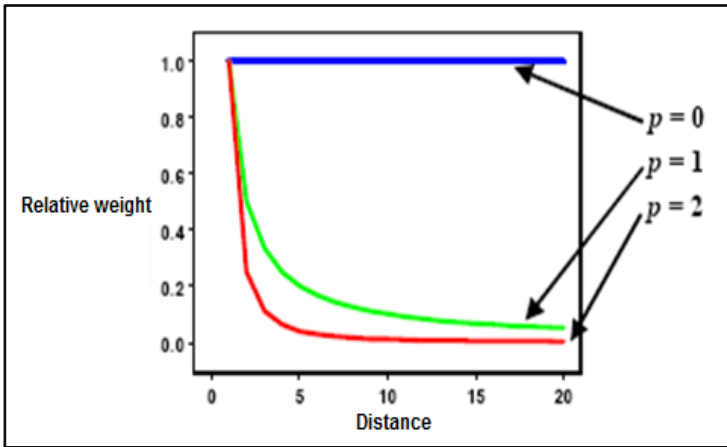


Figure 2-10: Decrease of weight with distance illustration (Esri, 2018)

Total of 174 field points was used for the control experiment. Forty (40) field points were excluded from creating the DTM and used as the reference to check the quality of the DTM estimated. The remaining field points (134) were used to generate the DTM using both interpolation algorithms. After creating the DTM, the validation points were loaded and used to extract the corresponding interpolated values from the DTM'S created. The arithmetic difference between the validation and interpolated elevation and root mean square error was the calculated as shown in Figure 2-11 below.

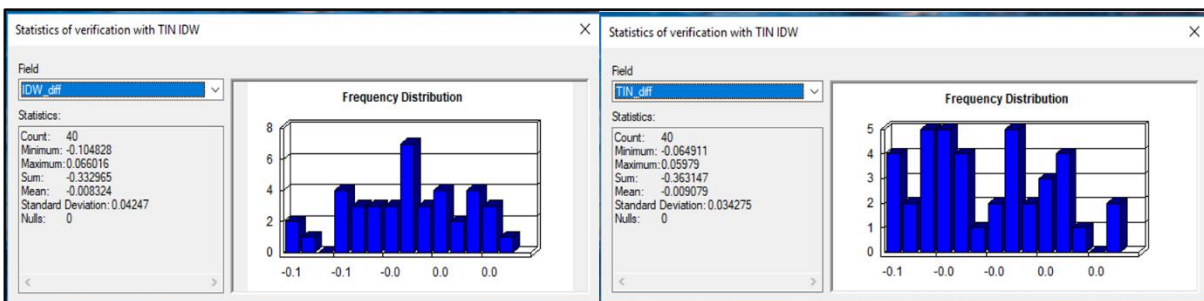


Figure 2-11: Statistics of IDW and TIN interpolation

From Figure 2-11 above, most of the arithmetic difference for TIN is 0, unlike IDW difference. Also, the root mean square error (RMSE) was 0.04m and 0.01m for IDW and TIN respectively. Hence, TIN interpolation algorithm was used for generating the DTM for all blocks.

#### 2.6.4. UAV DTM accuracy assessment

The positional accuracy of the generated UAV-DTM error was assessed by comparing the DTM values to field points (reference). The boundary of each canopy density class was used to extract the corresponding DTM. The extracted DTM values were then compared to the field points measured during the topographic survey to obtain the error. From the errors, the root mean square error (RMSE), mean error (ME), and standard deviation (SD) were calculated with the assumption that the errors are normally distributed.

The root mean square error and mean error was used to evaluate the error in the UAV DTM generated while standard deviation was used to determine the distribution of the error. Equations 1a – 1d below shows the various formulae used.

$$X_i = P_i - O_i \quad (\text{Eq. 1a})$$

$$ME = \frac{1}{n} \sum_{i=1}^n X_i \quad (\text{Eq. 1b})$$

$$RMSE = \sqrt{1/n \sum X_i^2} \quad (\text{Eq. 1c})$$

$$SD = \sqrt{\sum(X_i - \bar{X})^2/n} \quad (\text{Eq. 1d})$$

where

$X_i$ = error in elevation

$P_i$ = predicted value (UAV DTM)

$O_i$ = observed values (field point)

RMSE = root mean square error

ME = mean error

SD = standard deviation

n = number of observations

The assumption of normal distribution of error is not always valid as the canopy density may have different influence on the points generated. Due to this, the elevation error was tested to determine if it is normally distributed or not. The quantile-quantile (Q-Q) and histogram plots were used to determine the normality of the error. The Q-Q plot is a graph of the empirical distribution function versus the normal distribution of theoretical quantile (Ford, 2015). If the distribution is normal, the Q-Q plot falls on the straight line produced. The deviation of the distribution from the straight line gives an indication of the non-normality of the data.

If the error is normally distributed, the RMSE calculated will be accepted as the RMSE value as the assumption is valid. However, if the error is not normally distributed, robust accuracy measures such as normalized median absolute deviation (NMAD) will be used. The normalized mean absolute deviation was suggested because it is more resilient to outliers (Fras et al., 2016). The equation below is the formula for the normalized median absolute deviation.

$$NMAD = \text{median } |X_i - \bar{X}| \quad (\text{Eq. 2})$$

where

NMAD = normalized median absolute deviation

$X_i$  = error values

$\bar{X}$  = median of error

The percentile corresponding to the NMAD value obtained will then be determined. If the percentile is less than 95%, the corresponding 95% values will be deduced as the RMSE value since 95% is more reliable statistically. Hence the values corresponding to the 95% will be accepted as the root mean square error provided the error is not normally distributed.

To determine if the field point elevation and the corresponding UAV elevation was statistically different, the t-test was used. There are three ways to use t-test namely equal mean t-test, equal variance t-test, and unequal variance t-test. To determine which one is appropriate for any dataset, the F test was used to determine if the two samples have equal variance at an alpha of 0.05 (95% confidence interval). After determining the type of t-test to used, the appropriate t-test was implemented also at 95% confidence interval.

#### 2.6.5. Canopy height model (CHM) generation

The Digital Surface Model and Digital Terrain Model generated from UAV processing and Digital Terrain Model generated from field points were imported into ArcMap. The raster calculator function was used to generate the



canopy height model (CHM) by finding the arithmetic difference between DSM and DTM. CHM based on both field point and UAV was estimated using the equations below.

$$\text{CHM}_{\text{UAV}} = \text{DSM}_{\text{UAV}} - \text{DTM}_{\text{UAV}} \quad (\text{Eq. 3a})$$

$$\text{CHM}_{\text{field point}} = \text{DSM}_{\text{UAV}} - \text{DTM}_{\text{field point}} \quad (\text{Eq. 3b})$$

where

$\text{DSM}_{\text{UAV}}$  = UAV Digital Surface Model

$\text{DTM}_{\text{UAV}}$  = UAV Digital Terrain Model

$\text{DTM}_{\text{field point}}$  = Field point Digital Terrain Model

$\text{CHM}_{\text{UAV}}$  = UAV derived canopy height model

$\text{CHM}_{\text{field point}}$  = Field point derived canopy height model

The CHM was used as input to extract tree height.

#### 2.6.6. Crown projection area (CPA)

Research shows that there is a relation between crown projection area and DBH hence CPA can be used as a DBH proxy in a plantation forest but can be complicated in the tropical forest due to multiple tree height (Song et al., 2010; Hirata, Tsubota, & Sakai, 2009). During the fieldwork, a minimum of 63 biometric data (DBH and tree height) per canopy density class was measured to develop a model between DBH and CPA.

Some methods have been used to estimate crown projection area however the digitizing option was chosen in this study because the real shape of the tree crown, as accurate as possible, was required. Other studies used Object-based Image Analysis (OBIA) to estimate the crown projection area. Although OBIA can be used to generate tree crown for a large area at a reasonable accuracy depending on the segmentation algorithm used, this research does not aim to compare segmentation algorithms.

The tree crowns of different shape and species that were easily identified in the orthophoto were digitized using ArcMap. When tree crown was not readily observable due to the intermingling effect, the calculated canopy height model was added to aid in identification using the swipe function. Also, the individual UAV images assisted in identification and delineating the tree crowns.

#### 2.6.7. CPA-DBH relation

The research aims to estimate aboveground carbon for trees in each canopy density class using allometric equations. DBH of trees is one of the inputs used in the allometric equation however not all tree DBH was measured on the field during the field work. The DBH and CPA were used as input to develop a mathematical model that can be used to predict DBH from CPA as the CPA was extracted from all the trees within the canopy density class. Before the model was developed, the area of the CPA was calculated.

To determine the relation between the digitized CPA and field-measured DBH, a scattered plot was plotted and four trend line (linear, quadratic, exponential, and logarithmic) fitted. The four-trend line was tested to determine which one gave a better prediction by assessing the relation between CPA and DBH using the R-square value, prediction equation (to determine the accuracy of the predicted values), and RMSE to quantify the prediction errors. The best model was then used to predict the DBH.

#### 2.6.8. Individual tree height extraction

The crown projection area digitized from the orthophoto represents individual trees on the ground. The tree height can be extracted from the canopy height model however the canopy height model shows different elevation values

within individual crown projection area which represents individual trees. Since trees grow towards the sun, the highest canopy height model value within each crown projection area was extracted and used as tree height. The highest values were extracted using the zonal statistics tool in ArcMap. Two canopy height model values were calculated, one based on UAV data and the other based on field point data. The tree height estimated from these two canopy height models were then compared to tree height retrieved from a yield model and tree height measured on the field.

### 2.6.9. Estimating aboveground carbon

Tree height was estimated from UAV-CHM and field-CHM while DBH was measured/modeled. With the DBH and tree height, aboveground biomass was modeled using an allometric equation. The study considered a teak plantation and riparian forest hence two allometric equations were used for the two forest types. The allometric equations proposed by Polinder (2016) was used to estimate the AGB for the teak plantation while Chave et al. (2014) was used to estimate AGB for the riparian forest. Equation 4 below is the allometric equation used.

$$\text{aboveground biomass (Polinder, 2016)} = 0.0159 + 25.752e^{-6}D^{2.142}H^{0.902} \quad (\text{Eq. 4a})$$

$$\text{aboveground biomass (Chave et al., 2014)} = 0.0673 * [p * D^2H]^{0.976} \quad (\text{Eq. 4b})$$

From equations 4a and 4b above, aboveground biomass was estimated per tree for each canopy density class. The aboveground carbon was subsequently estimated from the aboveground biomass using the conversion factor propose by IPCC (2006) which states that about 47% of aboveground biomass is aboveground carbon. The total aboveground carbon per hectare was then calculated.

## 2.7. Data analysis

Data analysis was carried out using Excel 2016 and R software to test the proposed hypothesis, answer the research questions, and achieve the stated objectives of the study. The statistical analysis employed for data analysis are histogram, descriptive statistics, RMSE, correlation, and t-test.

The descriptive statistics and histogram were used to get an overview and graphic description of the field measured DBH. The RMSE was calculated to quantify the overall error of UAV-DTM under different forest canopy density. A scatter plot with trend line was used to establish the mathematical relationship between the CPA and DBH. The t-test which can be used to determine if there is a significant difference between two variables at a specified confidence interval was used to compare tree height from field point and UAV. Also, the t-test was used to compare aboveground carbon estimated from UAV and field point estimated tree height.

### 3. RESULTS

Below are the results of the data processing. All maps produced are in Universal Transverse Mercator (UTM) coordinates system.

#### 3.1. Biometric data

The diameter at breast height was measured for 294 trees divided over the four canopy density classes. The DBH of all measured trees and per canopy density class was summarized using descriptive statistics to get a general overview of the data. Table 3-1 below shows the descriptive statistics.

Table 3-1: Summary of descriptive statistics of measured DBH

	Number	Minimum (cm)	Maximum (cm)	Mean (cm)	Standard deviation	Skewness
DBH (open)	76	14.9	25.2	20.2	2.2	0.1
DBH (medium)	74	16.3	29.2	22.1	3.1	0.5
DBH (dense)	81	17.6	31.6	24.6	3.3	0.4
Riparian	63	10.4	58.6	21.4	9.8	2.3
DBH (all trees)	294	10.4	58.6	22.1	5.5	2.5

The descriptive statistics above shows that the DBH in the plantation (open, medium and dense canopy) forest was between 14.9 to 31.6 cm while the DBH range for the riparian forest was 10.4 to 58.6 cm. Also, skewness which gives an idea of the nature of data distribution shows that open, medium and dense (plantation) canopy have DBH which is normally distributed and slightly positively skewed while the skewness of the riparian canopy indicate the data is not normally distributed but positively skewed. The standard deviation, which indicates the spread in the data, shows that the DBH of trees in the plantation forest does not differ much unlike the riparian forest which has a standard deviation of 9.8. From the mean of the dataset, the trees mostly had DBH between 20 to 25 cm.

The get a pictorial view of the distribution of the data, histogram and the associated distribution of the data was plotted as shown in Figure 3-1 below.

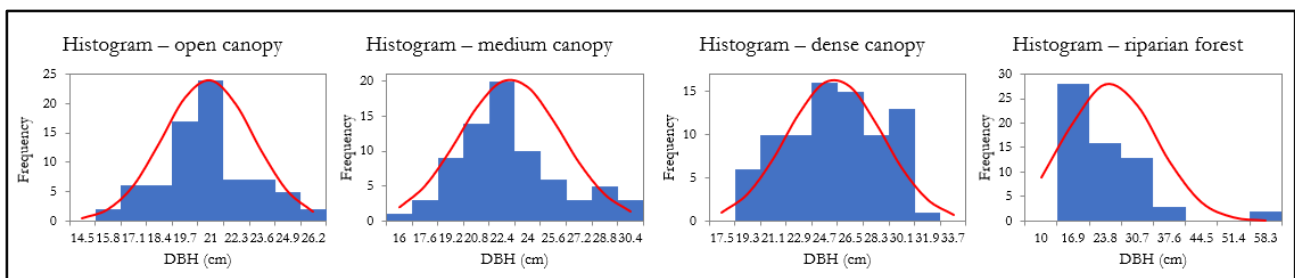


Figure 3-1: Histogram and normal distribution curve of measured DBH

From Figure 3-1 above, it seems DBH in open, medium, and dense canopy are normally distributed unlike DBH in riparian forest. The Shapiro Wilk statistical normality test at 95% (alpha of 0.05) confidence interval was performed to determine the normality of the measured DBH and the result shown in Table 3-2 below.

Table 3-2: Result of Shapiro significance test

Canopy density	DBH (open)	DBH (medium)	DBH (dense plantation)	DBH (dense riparian)
Significance	0.17	0.14	0.09	0.02

Since the normality test was at 95% confidence, all values greater than 0.05 implies that the measured DBH are normally distributed. From Table 3-2 above, the data in the open, medium, and dense canopy density are normally distributed since the significant values are greater than 0.05 unlike the DBH data in the riparian indicating that the DBH in the riparian is not normally distributed.

### 3.2. Field point result

From the control experiment that was carried out to determine which interpolation algorithm to use, the triangulated irregular network (TIN) interpolation algorithm was used to generate the field point DTM. From the field points obtained, 248 and 194 field points were used to generate the DTM for block 1 and 2 respectively and the result shown in Figure 3-2 below.

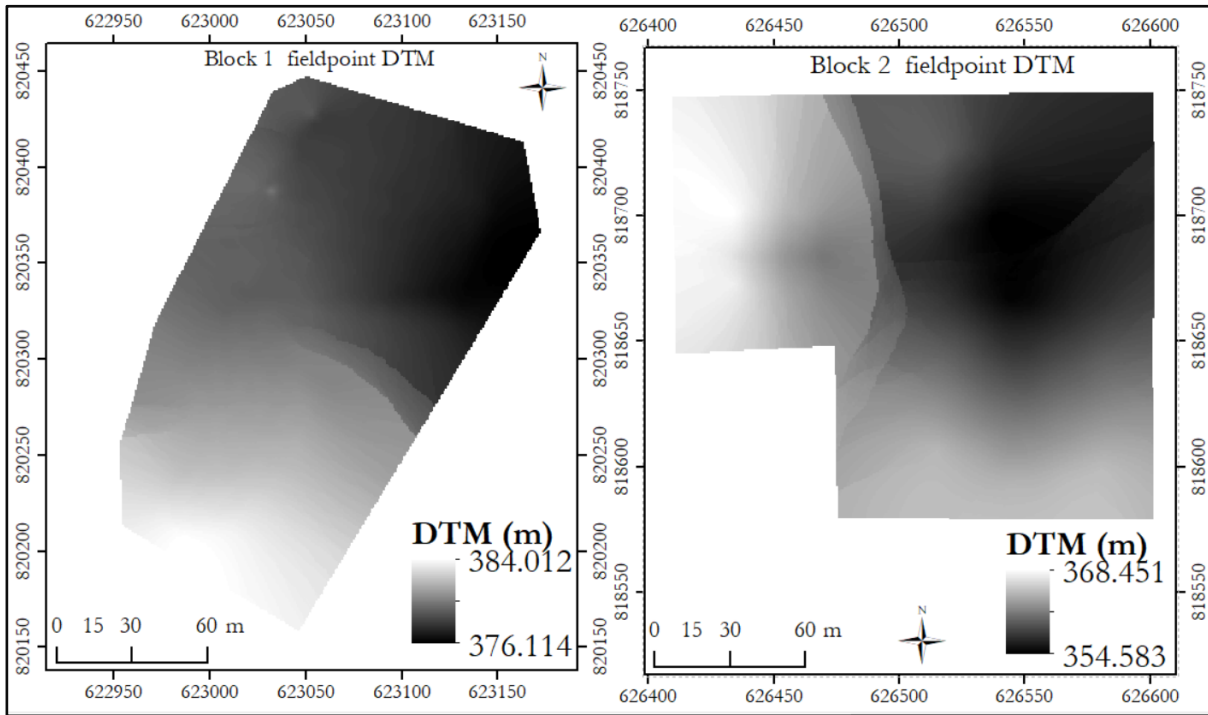


Figure 3-2: DTM generated from field points

From Figure 3-2 above, it can be seen that the DTM range is 376 to 384 m for block 1 and 354 to 368 m for block 2, indicating that block 2 is in a low area compared to block 1. There are no abrupt changes in the elevation for block 1, but there seem to abrupt changes in block 2 (from upper left to upper right).

### 3.3. UAV processing result

The Digital Terrain Model, Digital Surface Model, and orthophoto obtained from UAV image processing are shown in Figure 3-3 and 3-4 below.

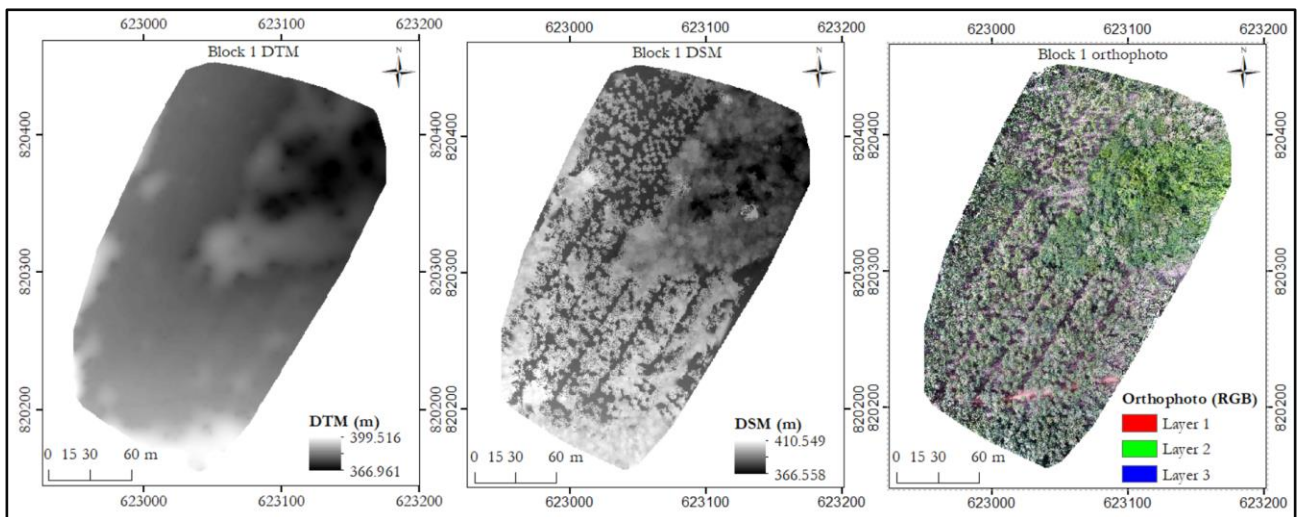


Figure 3-3: UAV result for block 1

Figure 3-3 above shows the DTM range of 367 to 399 m and DSM range of 366 to 410 m. The orthophoto shows the extraction line (middle) and road (lower part). The riparian forest is visible, though a bit blurred, probably due to intermingling crowns in the upper right while the open canopy is in the upper left corner. The medium canopy density is in the middle part of the orthophoto and clear crowns are visible on the DSM while the dense canopy is visible in the lower part of the orthophoto.

With the boundary of block 2 used for the topographic survey, the corresponding boundary was extracted from the UAV results and shown in Figure 3-4 below.

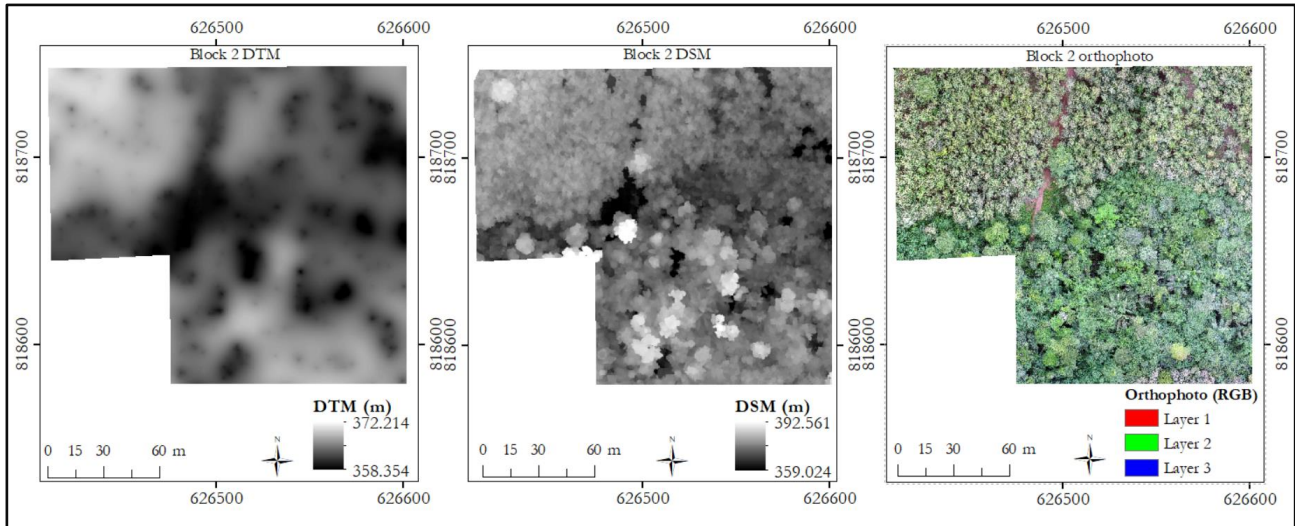


Figure 3-4: Photogrammetric result for block 2

Figure 3-4 above shows the DTM range of 358 to 372 m and DSM range of 359 – 392 m. The orthophoto also shows the riparian is located in the lower section while the dense is found in the upper section of the orthophoto. A road can also be observed in the middle of the orthophoto.

To get an overview of the point clouds used to generate the DTM, DSM, and orthophoto, a section of the report generated after processing the UAV images is shown in Table 3-3 below.

Table 3-3: UAV image processing information.

Name	Images used	Coverage (hectares)	Point cloud	Point density (point/ m <sup>2</sup> )	RMSE (m)
Block 1	465	5.63	102,830,395	134	0.26
Block 2	247	2.79	30,997,857	108	0.34

From Table 3-3 above, block 1 had higher point density than block 2. Also, the georeferencing RMSE for block 1 was better than that of block 2 because block 1 had more open spaces making it possible to properly distribute the GCP hence improving the georeferencing root mean square error.

### 3.4. Accuracy assessment of UAV DTM

After generating the DTM for each UAV block, the accuracy of the generated DTM was assessed by comparing with the field points obtained during the topographic survey. The root mean square error (RMSE), mean error (ME), and standard deviation (SD) were computed for each canopy density class under the assumption that the error is normally distributed and the result shown in Table 3-4 below.

Table 3-4: UAV DTM accuracy assessment

Canopy density class	Open	Medium	Dense (plantation)	Dense (riparian)
RMSE (m)	1.05	1.3	1.7	3.8
Mean error (m)	0.57	0.76	-1.1	-1.6
Standard deviation	0.88	1.09	1.28	3.46

From Table 3-4 above, the open canopy has the lowest RMSE while riparian has the largest RMSE. It can also be observed that RMSE increases with the canopy density. Also, open and medium canopy density have a positive mean error while dense (both plantation and riparian) have negative mean error which imply most of the UAV-DTM was underestimated in the dense and riparian canopy. The standard deviation of the error also increased with the canopy density with the lowest and highest been open and dense riparian class.

To test the validity of the assumption that the errors are normally distributed, quantile-quantile (Q-Q) plots were used as shown in Figure 3-5 below.

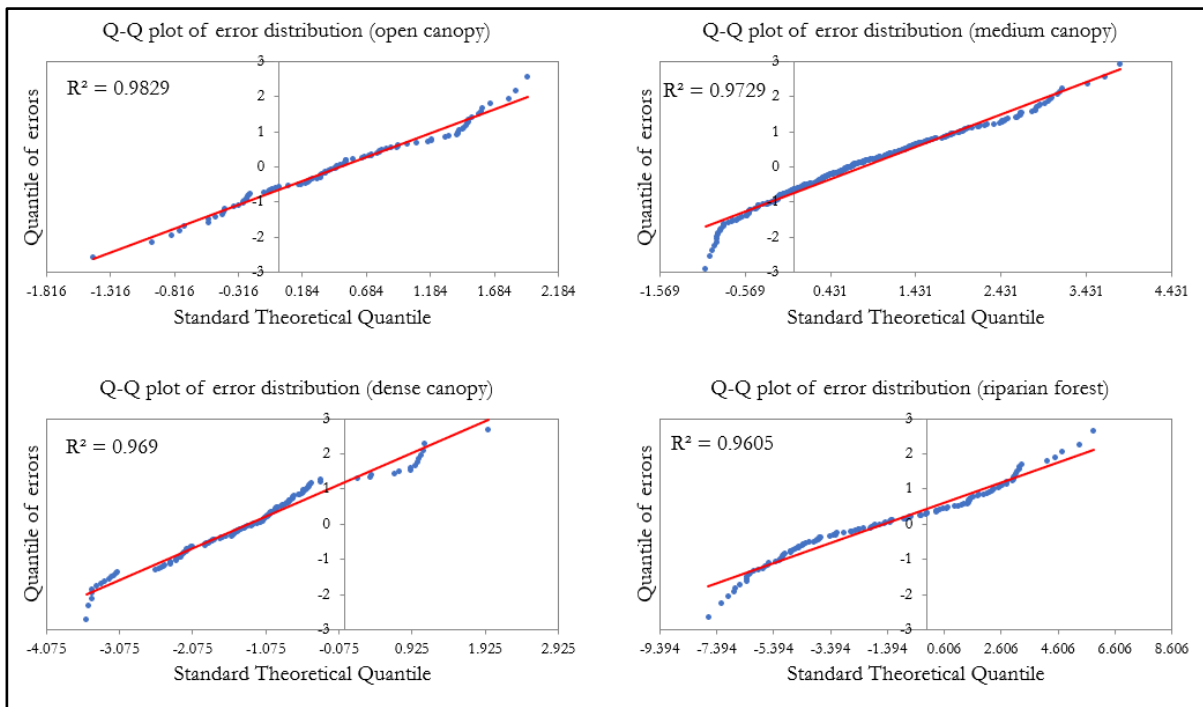


Figure 3-5: Q-Q of errors per canopy density class

From the Q-Q plot, the errors follow the theoretical values which results in high R-square values. The R-square value explains to what extent the variance of one variable explains variance of the other variable (Nagelkerke, 2008). While open canopy has the highest R-square, riparian canopy has a relatively small R-square implying that the error in the open canopy is similar to the theoretical quantile than errors in the riparian forest. From the R-square values in Figure 3-5 above, the errors were normally distributed. Hence it was appropriate to use RMSE to quantify the error in UAV generated DTM.

After quantifying the error, the next step was to determine if there was any difference in UAV and field point elevation and this was executed using the t-test. Prior to the t-test, F test was used to determine if the two samples (field point and UAV elevation) have equal variance at an alpha of 0.05 (95% confidence interval) and the result shown in Table 3-5 below.

Table 3-5: F-Test Two-Sample for Variances

	Open canopy	Medium canopy	Dense canopy	Riparian forest
F	0.910041736	0.645069	1.377784	0.024091
P(F<=f) one-tail	0.320002262	0.215314	0.008414	0
F Critical one-tail	0.717328593	0.821823	1.246413	0.745143

From Table 3-5 above, P(F<=f) is greater than 0.05 for open and medium canopy inferring that the two samples (UAV and field-measured elevation) have equal variance. For dense canopy and riparian forest, P(F<=f) is less than 0.05 which suggests that UAV and field measured elevation have unequal variance. From the F-test result, t-test with equal variance was used for open and medium canopy while t-test with unequal variance was used for the

dense canopy and riparian data. At 95% confidence interval, the t-test was executed and the result shown in Table 3-6 below.

Table 3-6: t-Test result

	Open canopy	Medium canopy	Dense canopy	Riparian forest
t Stat	-0.62319204	-0.94923	-0.93652144	4.689075794
P(T<=t) one-tail	0.266937753	0.354110247	0.425243654	3.37781E-06
t Critical one-tail	1.652585784	1.647559815	1.648347961	1.65647927
P(T<=t) two-tail	0.533875506	0.425874252	0.400321458	6.75562E-06
t Critical two-tail	1.972017478	1.964179027	1.965407333	1.978098842

The t-test works with the null hypothesis that there is no significant difference in the test sample (field and UAV height). From t-test result above, P(T<=t) is greater than 0.05 for the open, medium, and dense canopy which implies that the field point elevation is not different from the corresponding UAV elevation. Hence the null hypothesis cannot be rejected for open, medium, and dense canopy densities. However, P(T<=t) is less than 0.05 for riparian canopies which infers the field point elevation is different from the corresponding UAV elevation. Hence the null hypothesis was rejected.

The UAV-DTM accuracy assessment answered research question 1 which is to estimate the accuracy of DTM generated under the four-canopy density class.

### 3.5. Canopy height modeling per UAV block

After obtaining the required output (Digital Surface Model and Digital Terrain Model), the canopy height model (CHM) was generated. Two canopy height models were generated for each UAV blocks, one from UAV data (UAV DSM and DTM) and the other field data (UAV DSM and field point DTM).

Canopy height model represents the height of the tree and since trees cannot have negative height, all canopy height model values below 0 were reclassified as 0. Figure 3-6 below is the result of block 1 canopy height models.

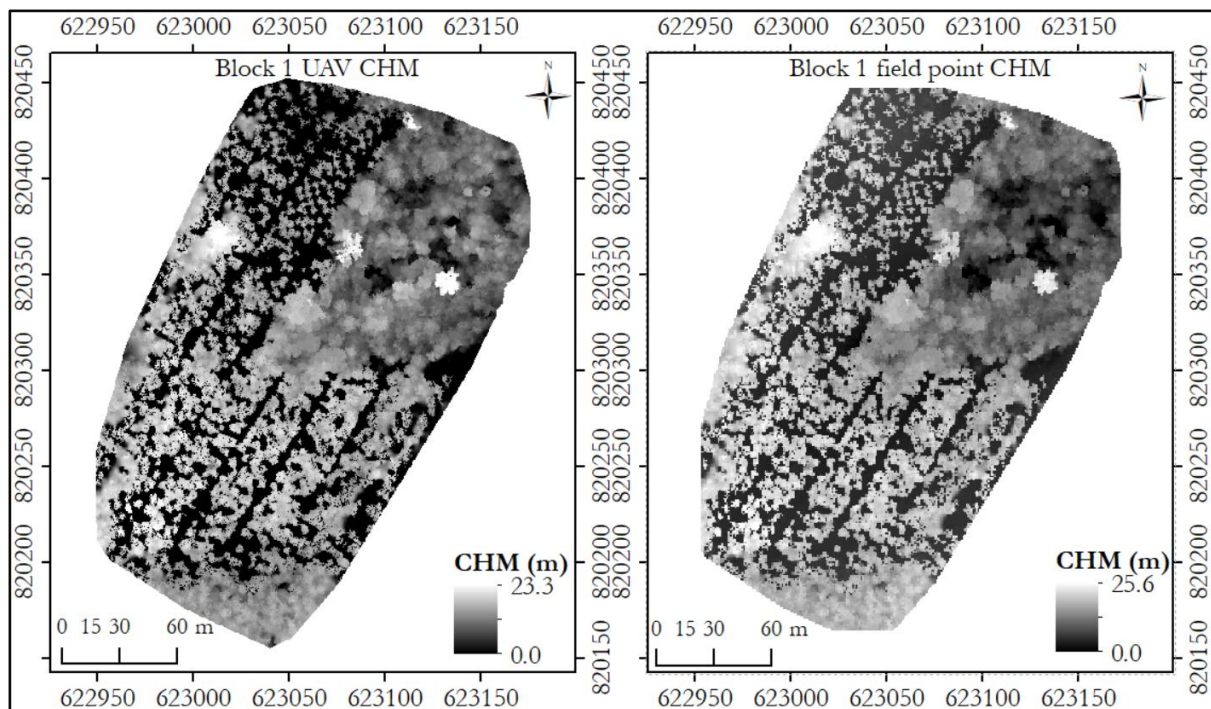


Figure 3-6: UAV and field point derived CHM for block 1.

From Figure 3-6 above, the highest tree height according to the UAV and field canopy height models are 23.3m and 25.6m respectively. The lowest values represent the bare ground and is in accordance with what was observed on the field.

Figure 3-7 below also shows the result of block 2 canopy height models.

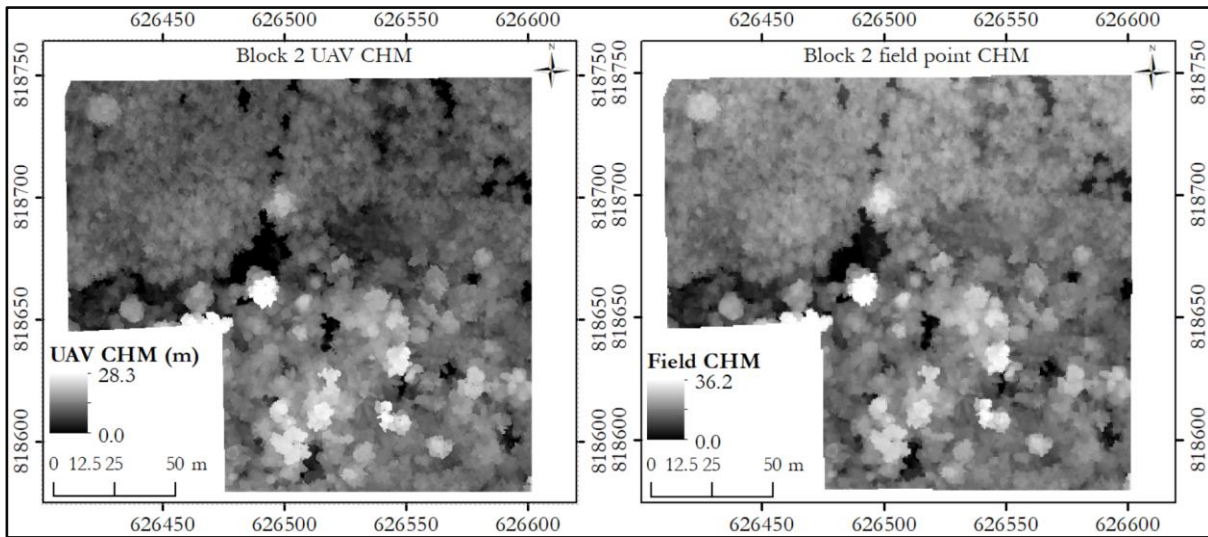


Figure 3-7: UAV and field point derived CHM for block 2.

From Figure 3-7 above, the highest tree according to the UAV-CHM and field points are 28.3m and 36.2m respectively. The lowest canopy height models were the open space and road (middle) in the study area.

The calculated canopy height models had some negative values and this could be attributed to underestimation of the UAV DSM due to the presence of a felled tree, shrubs, or debris on the ground. Also, overestimation of DTM due to branch or leaves covering the soil could result in negative values for the estimated canopy height model. On bare soil, DTM and DSM would have almost the same value. However, the felled trees would reduce UAV derived values because the light ray does not hit the ground but the felled tree.

### 3.6. Crown projection area (CPA)

Digitizing of tree crown resulted in the generation of crown projection area (CPA) that were representative of the tree as shown in Figure 3-8 below.

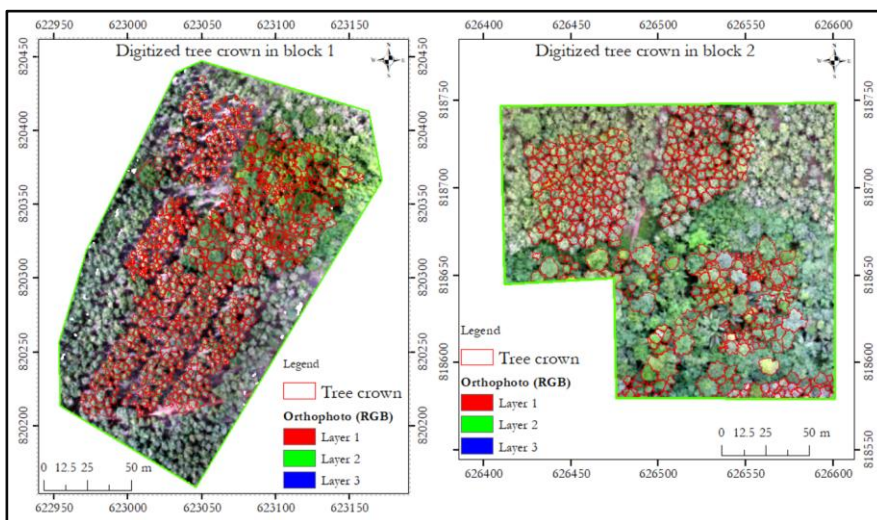


Figure 3-8: Digitized tree crown in block 1 and 2



The digitized CPA with its associated DBH was used to develop a mathematical model that predicts DBH from CPA.

### 3.7. Tree height per canopy density class

With the digitized crown projection area and canopy height models, the tree height was estimated from UAV and field point data per canopy density class and the result shown in Figures 3-9 and 3-10 below.

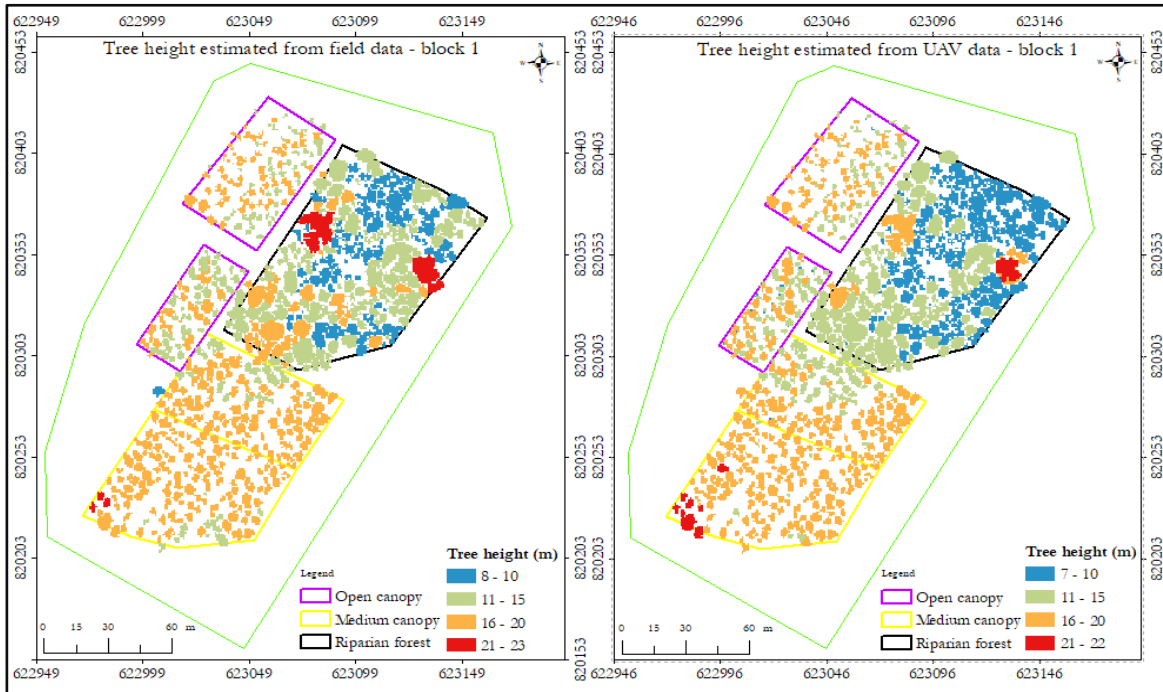


Figure 3-9: Tree height estimated from UAV and field data for block 1

From Figure 3-9 above, there are some difference in tree height estimated from UAV and field point data. Although there are differences in tree for every canopy density, the riparian forest shows the most difference in tree height estimated. According to UAV tree height, some trees in the upper left of the riparian are between 7 to 10m while those trees have height between 11 to 15m according to field point tree height. The lower part of the medium class has some tree height classified to be between 16 to 20m when estimated from field data but are between 21 to 22m for tree height estimated for UAV data. Figure 3-10 is the tree height estimated for block 2.

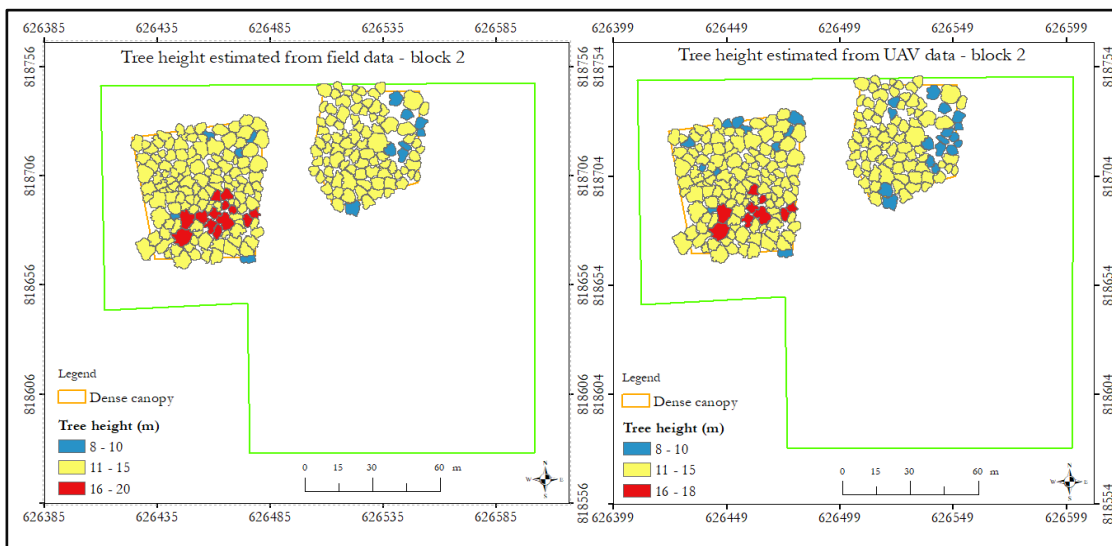


Figure 3-10: Tree height estimated from UAV and field data for block 2

From Figure 3-10 above, not much difference in the tree height estimated from UAV and field point data can be observed. However, the left side of the dense canopy shows trees with height between 8 and 10m according to the UAV data but those trees have height between 11 and 15m according to the field data.

To compare the tree height estimated from UAV and field point data, the average height of tree was calculated. Although the tree height measured with the clinometer has error (section 2.5.5), the data can give an indication of the average height of the measured tree height. Table 3-7 below shows the mean height per trees in canopy density class.

Table 3-7: Average tree height per canopy density class

Average height (m)	Open canopy			Medium canopy			Dense canopy			Riparian forest		
	UAV-based	Field point-based	Suunto-based	UAV-based	Field point-based	Suunto-based	UAV-based	Field point-based	Suunto-based	UAV-based	Field point-based	Suunto-based
	13.6	14.3	14.1	14.2	15.3	14.9	16.1	16.9	16.7	11.6	15.8	16.1

From Table 3-7 above, the tree height estimated from UAV and field CHM is almost the same as tree height measured with the clinometer in the open canopy, medium canopy, and dense canopy. However, the UAV tree height of trees in the riparian forest is about 4m below the height of trees estimated by the field point CHM and the clinometer.

To determine if the difference in tree height is significant, the t-test was used at a confidence interval of 95%. Before the t-test, the F test was first executed to determine if the data has equal variance and the result is shown in Table 3-8 below.

Table 3-8: F test for tree height per canopy density

	Open canopy	Medium canopy	Dense canopy	Riparian forest
F	1.22642265	0.916175822	0.917349411	1.423173258
P(F<=f) one-tail	0.18781656	0.232575873	0.267715516	0.001804243
F Critical one-tail	1.46188457	0.820956087	0.795188171	1.220284182

From Table 3-8 above, P(F<=f) is greater than 0.05 for open, medium, and dense canopy hence the height of trees from UAV and field data have equal variance. However, P(F<=f) is less than 0.05 for trees in riparian forest hence UAV and field measured elevation have unequal variance. From the F Test, t-test with equal variance at an alpha of 0.05 was used for open, medium, dense canopy while t-test with unequal variance at 95% confidence interval was used for riparian forest and the result shown in Table 3-9.

Table 3-9: t-test of tree height per canopy density class

	Open canopy	Medium canopy	Dense canopy	Riparian forest
t Stat	0.49938217	-0.042182521	0.502837481	-7.823209752
P(T<=t) one-tail	0.30911611	0.483184143	0.307672962	1.37095E-14
t Critical one-tail	1.65494017	1.647588963	1.648542529	1.647690825
P(T<=t) two-tail	0.61823223	0.966368285	0.615345925	2.74191E-14
t Critical two-tail	1.97569393	1.964224446	1.965710612	1.964383179

The null hypothesis for t-test states that there is no statistical difference between the UAV estimated tree height and field point estimated tree height. From Table 3-8 above, P(T<=t) is greater than 0.05 for the open, medium, and dense canopy, hence the null hypothesis cannot be rejected for open, medium, and dense canopies. This implies that tree height estimated from field point data is not different from tree height estimated from UAV data. However, P(T<=t) is less than 0.05 for riparian canopies. Hence the null hypothesis is rejected for the riparian forest implying tree height estimated from UAV and field point data is different.

From the result above, canopy density has a significant effect on tree height estimated from UAV and field point data in the riparian forest but the difference in tree height estimated from UAV and field point data is not statistically significant for the open, medium, and dense canopies at 95% confidence interval. This answered research question 3.

### 3.8. Crown projection area (CPA) and diameter at breast height (DBH) relation

The DBH measured was divided into their respective classes for the CPA-DBH model development and validation. The data per canopy density class was divided randomly in the ratio 60:40. Thus 60% of the data (DBH and associated CPA) was used for model development while the remaining 40% was used for model validation. Out of the four models developed per canopy density class, the model that performed best considering the R-square values are shown in Figure 3-11 below and the other three models are shown in Appendix 2.

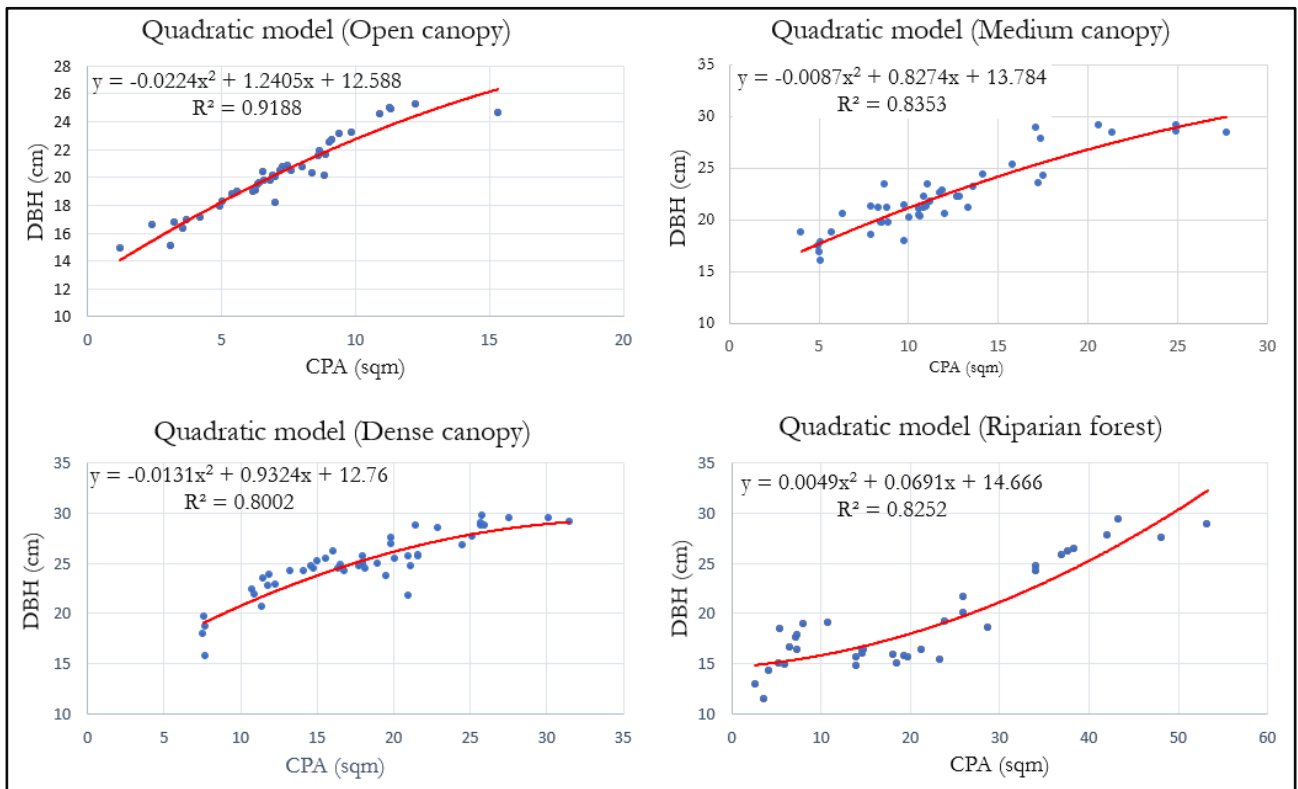


Figure 3-11: Model development result from each canopy density class

From Figure 3-11 above, quadratic models performed best for all the canopy density classes. Open canopy had the highest R-square and dense canopy had the lowest R-square.

Each of the models in Figure 3-11 above were used to predict DBH of the validation data. The predicted DBH was then compared to the field measured DBH to validate the model. RMSE was calculated to estimate the model error for DBH prediction and shown in Table 3-10 below.

Table 3-10: Model development result

Canopy density class	R <sup>2</sup>	RMSE (cm)
Open	0.9188	0.55
Medium	0.8353	0.943
Dense	0.8002	2.160
Riparian	0.8252	5.238

From the result in Table 3-9 above, the most errors in the prediction was in the riparian. Although there is more correlation between CPA-DBH of trees in riparian canopy than trees in dense canopy, the RMSE in riparian is

more than that of dense canopy. This suggests that how the data is selected for model development and validation influences the model developed.

For validation, a scatter plot through the origin between the model DBH and the field measured DBH (for all canopy density class) was plotted to also determine the correlation between the two parameters and the result is shown in Figure 3-12 below.

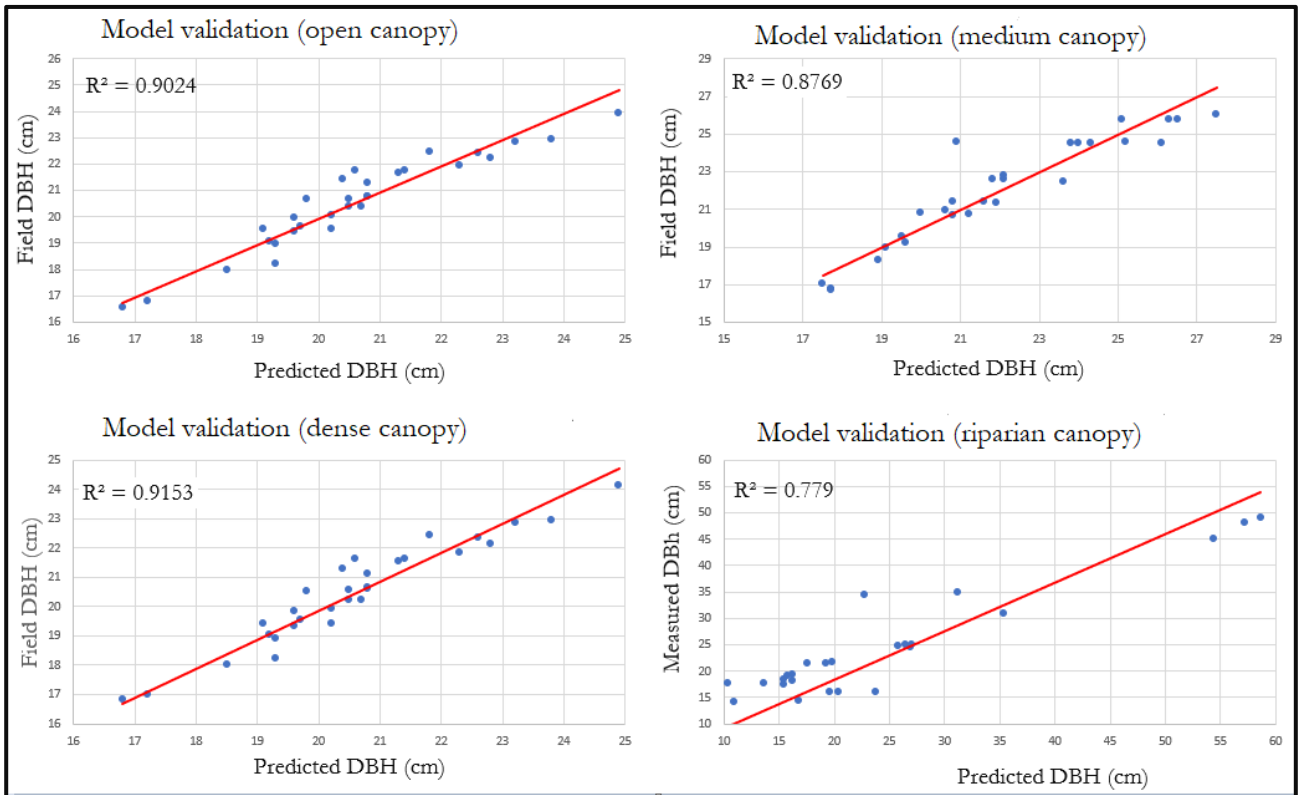


Figure 3-12: Linear regression through the origin between predicted and measured DBH per canopy density class.

From Figure 3-12 above, the dense canopy has the highest R-square for the validation model. As observed in Figure 3-11 and Table 3-9, while the R-square for riparian forest is more than that of dense forest, the RMSE of riparian is more than dense forest. This is further evident in the validation model as the R-square of dense (0.9153) is greater than the R-square of riparian (0.779).

The models developed and shown in Figure 3-11 were used to predict the DBH of trees that were not measured during the field. The relation developed answered research question 3.

### 3.9. Aboveground carbon estimation

Two aboveground carbon (AGC) was modeled using UAV-CHM and field-CHM for each canopy density class. Figures 3-13 and 3-14 below shows aboveground carbon for block 1 and 2 respectively.

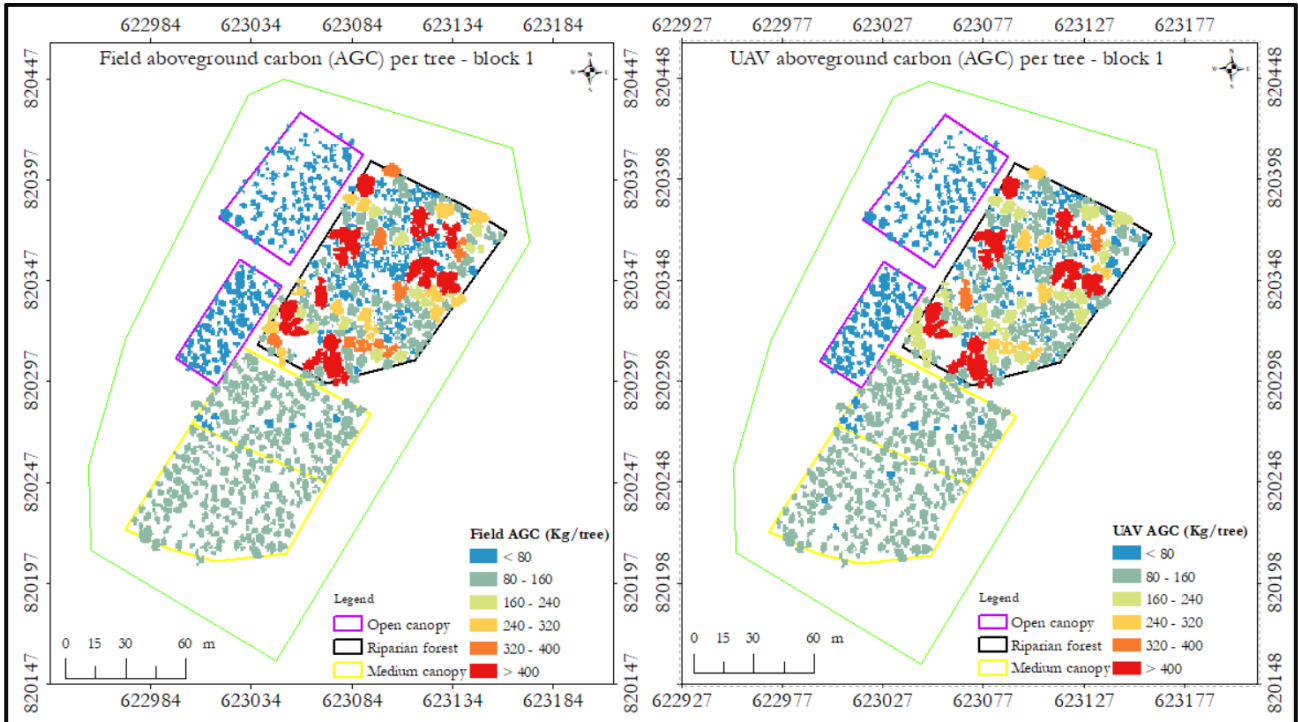


Figure 3-13: Block 1 aboveground carbon estimated from UAV and field data.

Figure 3-13 above shows there is not much difference in the AGC estimated from UAV and field CHM in the open and dense canopy unlike the riparian. The lower left and right of the riparian has trees whose aboveground carbon are estimated to be between 251 to 300 Kg and 301 – 350 Kg respectively according to the field data but estimated by the UAV to be between 151 – 200 Kg for the tree at the lower left and 251 – 300 Kg for the trees at the lower right of the riparian.

Figure 3-14 below shows the map of aboveground carbon estimated for block 2.

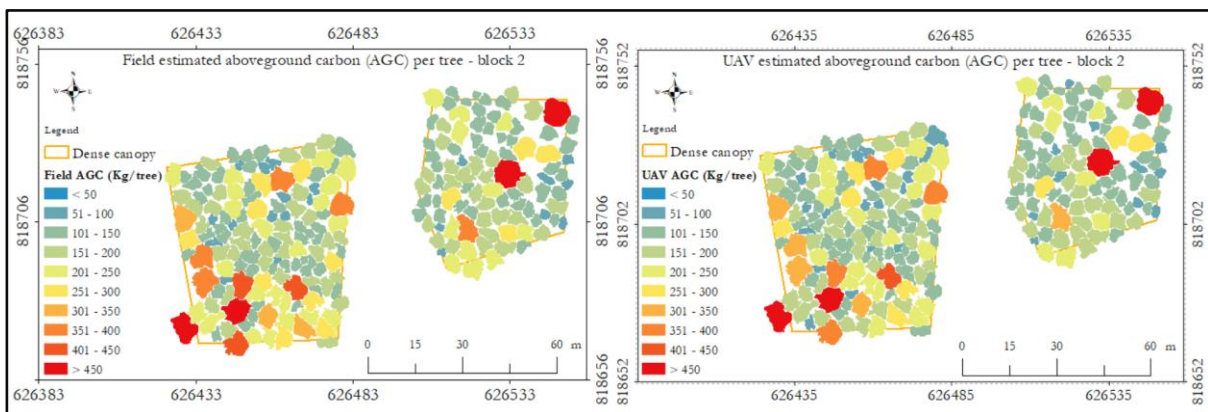


Figure 3-14: Block 2 aboveground carbon estimated from UAV and field data.

From Figure 3-14 above, there is not much difference in the aboveground carbon estimated from UAV and field data. However, a glance through the maps shows some little difference in the estimated aboveground carbon. For instance, looking at the lower left of the field estimated aboveground carbon map, some tree were estimated to have 201 to 250 Kg, but those trees were estimated to be between 151 to 200 from the UAV estimated aboveground carbon.

From the aboveground carbon estimated, the total aboveground carbon per hectare of canopy density class was calculated and the result shown in Table 3-11 below.

Table 3-11: Total aboveground carbon per hectare

Total aboveground carbon per hectare	Open canopy (9 years)	Medium canopy (11 years)	Dense canopy (11 years)	Riparian forest
UAV AGC (Mg/ha)	22.1	35.9	39.4	43.5
Field AGC (Mg/ha)	23.6	37.4	42.5	63.7

According to Table 3-11, riparian forest shows the most difference in total aboveground carbon estimated. While the field data estimated riparian forest total aboveground carbon per hectare as 63.7 Mg/ha, the UAV data estimated 43.5 Mg/ha as the total aboveground carbon per hectare

To determine if there is any significant difference in aboveground carbon estimated from UAV and field data, a t-test was used but F test was used to determine if the two samples (UAV-AGC and field-AGC) have equal variance at an alpha of 0.05 (95% confidence interval) and the result shown in Table 3-11 below.

Table 3-9: F-Test Two-Sample for Variances

	Open canopy	Medium canopy	Dense canopy	Riparian forest
F	1.004281281	1.091568083	0.861235467	0.731077251
P(F<=f) one-tail	0.488584381	0.249382719	0.214214505	0.012703783
F Critical one-tail	1.278706716	1.237653678	0.732878313	0.794297752

From Table 3-11 above, P(F<=f) is greater than 0.05 for open, medium and dense canopy classes hence the two sample (UAV and field AGC) have equal variance. However, the P(F<=f) is less than 0.05 for the riparian forest meaning the two sample have unequal mean.

The t-test with equal variance was then used to determine if the difference between the two samples (UAV-AGC and field-AGC) for open, medium, and dense canopy density are statistically significant at 95% confidence interval. For the riparian forest t-test with unequal variance at 95% confidence interval was used. Table 3-12 below shows the result of the t-test.

Table 3-10: Aboveground carbon t-Test result

	Open canopy	Medium canopy	Dense canopy	Riparian forest
t Stat	-1.034981511	0.49270254	-1.05779637	-1.991135439
P(T<=t) one-tail	0.150686138	0.311224511	0.145638809	0.023572906
t Critical one-tail	1.649097298	1.648047653	1.651623859	1.648671941
P(T<=t) two-tail	0.301372275	0.622449023	0.291277617	0.044145811
t Critical two-tail	1.96657546	1.964939272	1.970516243	1.965912343

From Table 3-12 above, P(T<=t) is 0.3, 0.6 and 0.2 for open, medium and dense canopy respectively which is greater than 0.05 indicating that there is no statistical difference in aboveground carbon estimated from UAV and field point in the open, medium, and dense canopy. Hence, the null hypothesis cannot be rejected in the open, medium, and dense canopy forest.

However, P(T<=t) for the riparian forest is 0.04 which is less than 0.05 indicating there is a statistical difference in AGC estimated from UAV and field data in the riparian forest which infers that there is a statistical difference in aboveground carbon estimated from UAV and field point in the riparian forest. Hence, the null hypothesis is rejected for riparian forest.

Estimating aboveground carbon for each canopy density class and testing the significance answered research question 4.

## 4. DISCUSSION

### 4.1. Distribution of biometric data (DBH)

The study area comprised of a teak plantation and riparian forest. The blocks established for this research contained the canopy density classes which had trees planted in 2008 and 2010. The planting year of the trees in the riparian forest is unknown. The trees in the open canopy were planted in 2010 while the trees in the medium and dense canopies were planted in 2008. Although it is expected that trees of the same species planted at the same year will have the same canopy density, this was not the case in the study area because of thinning. Thinning is a management practice that improves the growth of trees and can be defined as the removal of trees with less quality (Radio & Delgado, 2014). While the medium density class has been thinned twice (second thinning carried out in August 2018, a few weeks before the fieldwork), the dense canopy has been thinned once (almost 5 years ago). The thinning line can be observed as a strip of lines in Figure 3-3.

From the descriptive statistics (Table 3-1), the measured DBH was slightly positively skewed in the open, medium, and dense canopy density which are in the plantation forest but highly skewed in the riparian forest. The slight skewness could be because the trees in each canopy density was planted the same year hence there is not much variation in the DBH measured per canopy density. According to Doane & Seward (2011), the skewness of data is related to the mean, median, and mode as shown in Figure 4-1 below.

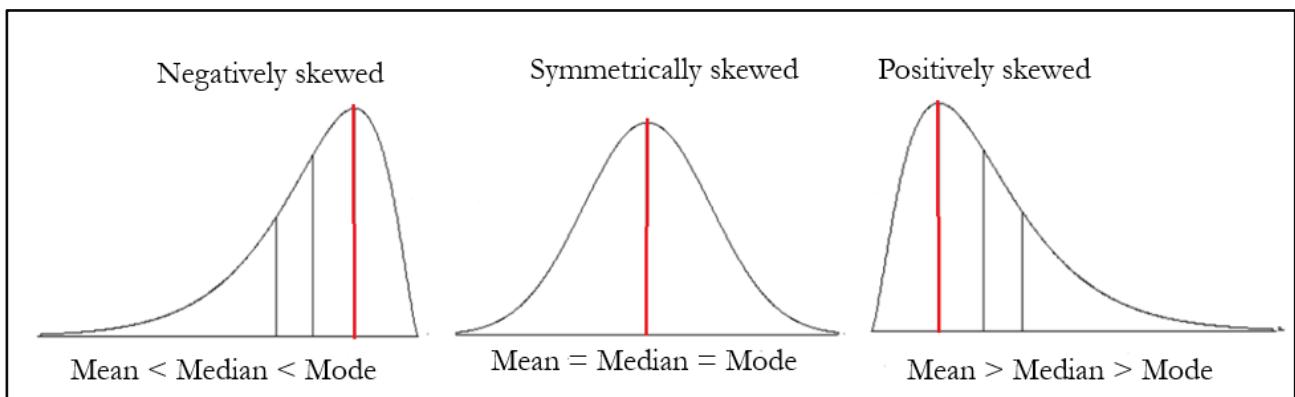


Figure 4-1: Relation between skewness, mean, mode, and median (Doane & Seward, 2011).

From Figure 4-1 above, for any data to be symmetrically skewed, the data should be normally distributed (on both sides) around the mean. With the mean as the central point, if the mean is greater than the median then the data is positively (right) skewed and vice versa. To determine if this relation exist for the measured DBH per canopy density, the mean and median is shown in Table 4-1 below.

Table 4-1: Mean and median per canopy density class

	Open canopy	Medium canopy	Dense canopy	Riparian forest
Mean	20.2	22.1	24.6	21.4
Median	20.1	21.5	24.4	18.5
Skewness	0.1	0.5	0.4	2.3

From Table 4-1 above, the mean is greater than the median for all canopy density classes which explains the positive skewness.

According to Table 3-1, the standard deviation (which express the spread of the data around the mean) is higher for the riparian forest than the other canopy density classes. The histogram of measured DBH in riparian forest (shown in Figure 3-1) shows that while most of the measured DBH is between 16 and 40 cm, there are some trees with DBH between 51 and 58.6 cm. The DBH variation is because the riparian forest unlike the plantation forest comprise trees of different species. These trees have different growth resulting in the variation of measured DBH.

The trees with big DBH (between 51 and 60 cm) are possible remnant of trees that remained after the area was deforested.

Very few studies have been carried out to determine establish growth models for teak in Africa. Akindele (1991) developed a growth index for teak in South-western Nigeria. Akindele (1991) proposed that a nine-year-old teak will have mean DBH range of 11-19 cm while a twelve-year-old teak will have DBH range of 17-23 cm. From Table 4-1, the mean DBH for the open canopy (which is about 9 years) is 20.2 cm while the mean DBH for the medium and dense canopy (which is about 11 years old teak) are 22.1 cm and 24.6 cm respectively. The difference in mean DBH between Akindele’s growth model and field measured DBH could be because of the different climate condition, soil type, and management practices which all influence growth of trees (Kaosa-ard, 1995).

#### 4.2. UAV-DTM accuracy assessment

The accuracy of DTM generated depends on the quality, quantity, and distribution of 3D points used (Nex, 2018a) which implies that if the data quality is poor, and few in quantity with bad distribution, the algorithm used to develop the DTM would not make any difference because the algorithm is just a tool that is used to interpolate the input values. According to Table 3-4, the RMSE calculated indicates that riparian forest has the most error. To quantify the errors in DTM, there is a need to identify where the errors are hence a map of UAV and field-point DTM is shown in Figure 4-2 below.

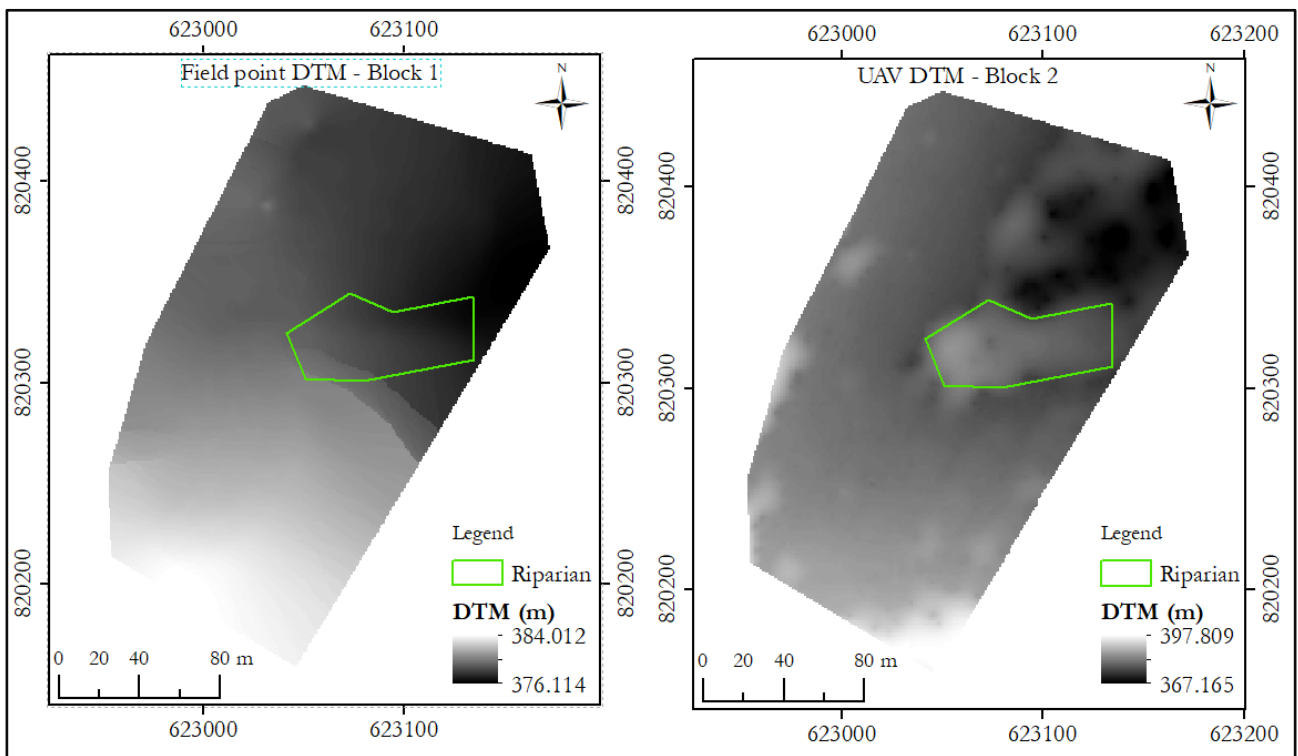


Figure 4-2: Field point and UAV DTM

From Figure 4-2, the terrain generally increases from the lower part to the top for the field point DTM, but the UAV DTM shows some undulations. Having a critical look at the riparian in both maps, the riparian in the field point DTM has low elevation while the riparian in the UAV DTM has high values. On the field, the lowest elevations were identified in the riparian unlike predicted by the UAV.

During the photogrammetric processing, random sample consensus (RANSAC), Bundle Block Adjustment (BBA), and gradual selection process improved the quality of the generated points (Esri, 2016a). These photogrammetric operations were implemented during the image processing to reduce the reprojection error and orient the images (Nex, 2018a). With the errors that can affect the quality of point reduced, other factors that can affect the DTM quality is the quantity and distribution of the points used to create the UAV-DTM.



To analyze the quantity of the points used to generate the DTM per canopy density, LAS points statistics was used to get a descriptive statistic of the points used to generate the DTM of each canopy. Also, the points per square meters were calculated to compare the point per canopy density generated. Table 4-2 below is the result of the point cloud statistics.

Table 4-2: Points statistics per canopy density class

Canopy class	Elevation (minimum)	Elevation (maximum)	Elevation (mean)	Point cloud count	Points per square meter
Open	378.54	383.166	380.735	749448	183
Medium	380.66	386.656	383.59	1279569	176
Dense	358.927	371.759	365.625	793281	154
Riparian	371.49	379.516	374.318	250596	34

According to Table 4-2, riparian has the least points per square meter while open canopy had the highest points per square meter. In general, the point generated decreased with increasing canopy density. The riparian forest has fewer points per square meter compared to the dense canopy plantation. Although both forest canopies are dense, the dense canopy class is a plantation forest with only teak trees planted while riparian forest has different tree species. Trees of the same species have similar growth provided they have the same conditions such as soil, rainfall, and temperature (Kaosa-ard, 1995). Also, since the plantation is monoculture, there is little undergrowth in the plantation, unlike the riparian forest where the undergrowth makes the canopy denser. Furthermore, since the trees are planted at a regular interval (about 3 by 3m) and the trees are thinned to improve its growth, there is little intermingling crowns in the plantation. However, in the riparian forest, the trees are planted at irregular interval which causes the canopy of the trees to be intermingled and further making the canopy dense. With limited undergrowth and intermingling crown effect, there is a reasonable probability of the UAV mirroring the forest floor in the plantation, unlike the riparian forest.

To quantify how the canopy density affects point density, the percentage decrease of points per canopy density was calculated with the assumption that if all canopy density was the same then the same or almost the same density of points will be generated. Table 4-3 below shows the decay of points per canopy density.

Table 4-3: Ground points percentage decrease

Canopy class	Point/square meter	Percentage decrease
Open	183	
Medium	176	3.8%
Dense	154	12.0%
Riparian	34	65.6%

The bar chart displays the percentage decrease in points per square meter for three canopy density classes. The y-axis is labeled 'Percentage decrease' and ranges from 0 to 70. The x-axis is labeled 'Canopy density class'. The bars are: Medium canopy (blue) at 3.8%, Dense canopy (orange) at 12.0%, and Riparian canopy (grey) at 65.6%.

From Table 4-3 above, points per square meter reduces by about 4% in medium and 12 % in dense canopy. However, the riparian forest had the most effect on the points generated.

To identify the distribution of the ground points, a map of ground point cloud per canopy density is shown in Figure 4-3 and Figure 4-4.

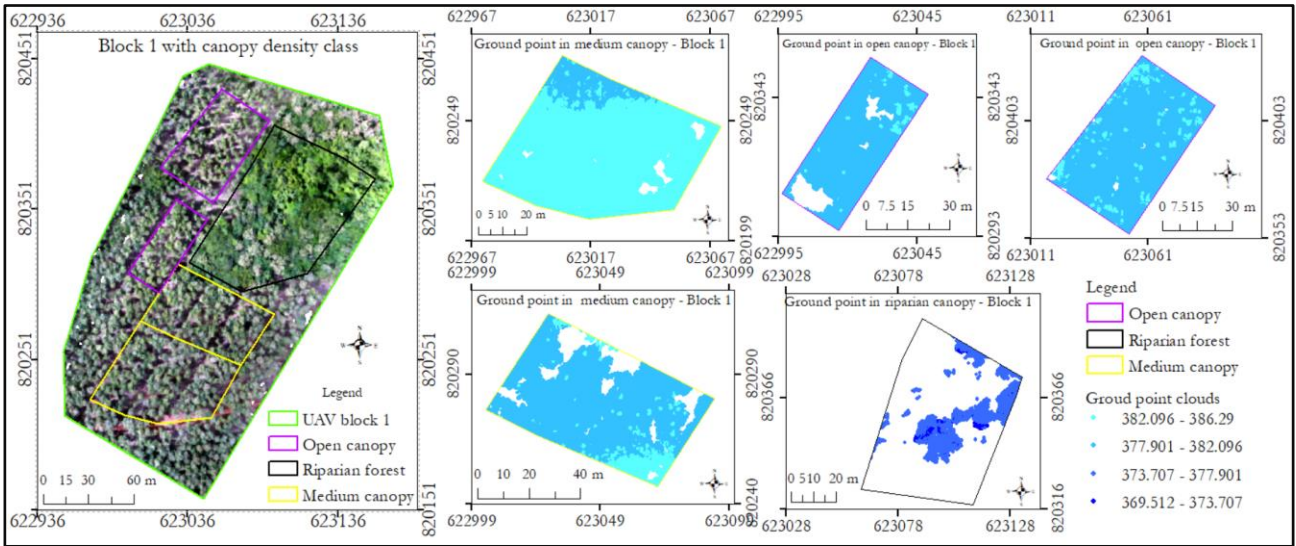


Figure 4-3: Points in block 1 canopy density

From Figure 4-3 above, both open and medium canopy have some section without ground points but this is a small section unlike the riparian forest where more than half of the area has no point clouds. Using an interpolation algorithm, the section without ground points can be assigned elevation values but the accuracy of any interpolation algorithm depends on the quality and distribution of points. In an area where the terrain has more details (such as an undulating area), the more points to use for the interpolation the better the terrain representation.

Figure 4-4 is the ground point in block 2.

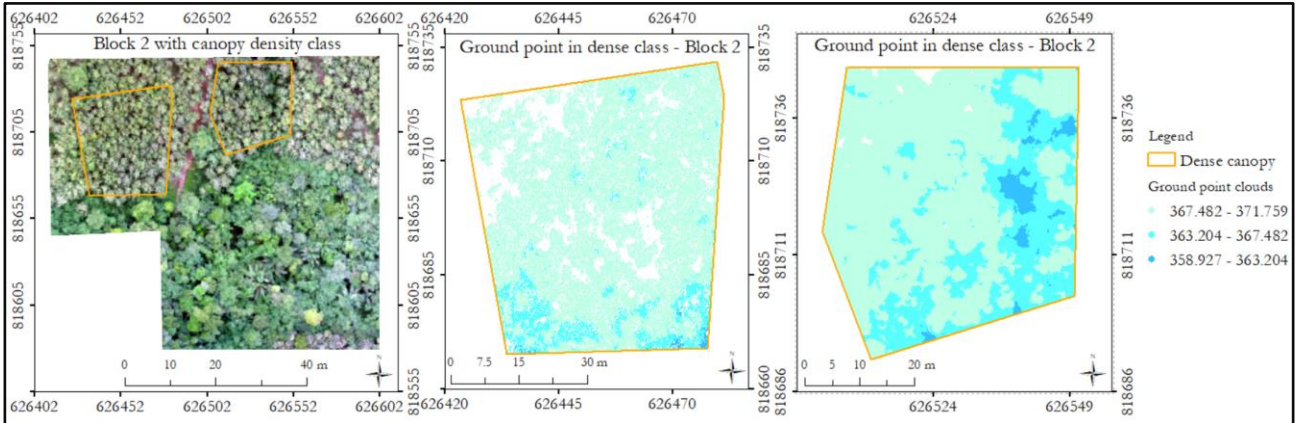


Figure 4-4: Points in block 2 canopy density

From Figure 4-4 above, ground points cover most part of the canopy hence a DTM which represents the terrain can be generated.

Figure 4-3 and 4-4, it can be observed that the ground points reduce as the canopy density increases. After assessing the quality, quantity, and distribution of the point clouds, the riparian forest affects the quality of DTM generated by UAV the most.

The result is comparable to Begashaw (2018) and Reuben (2017) who in their research indicated that points generated in the dense forest are less dense due to the inability of the UAV image to capture the ground resulting in errors in DTM generated. It is however interesting to notice that although dense canopy plantation and riparian forest are both dense, the riparian forest has the most effect on point generated.

Also, Debella-Gilo (2016) studied the accuracy of DTM generated under partly dense vegetation, a built-up area with complex topography and bare ground. Debella-Gilo (2016) concluded that the ground points does not deviate when compared to Airborne Laser Scanner (ALS) DTM except in dense forest canopies.

Furthermore, the result is similar to Balenović et al., (2016) who also studied the accuracy of UAV-DTM considering three mainland cover namely; grassland, forest, and shrub. In their research, Balenović et al., (2016) observed that although all the land cover they considered influence the quality of DTM, the complex nature of the land cover type yields the least accurate result.

#### **4.3. CPA-DBH relation**

The result obtained from CPA and DBH relation (Figure 3-11) shows that there is a positive relationship between CPA and DBH of trees which is significant. Out of the four models developed, quadratic models were chosen for all canopy density class. From the result, it can be observed that the R-square reduces as the canopy density increases. In the open canopy, the individual tree crown can be seen, hence improving the accuracy of the crown projection area (CPA) digitized resulting in the highest R-square for the model developed. In the medium and dense canopy densities, some tree canopies were intermingled, reducing the ability to identify and digitized the tree crown correctly. However, using the canopy height model and individual images improves the digitizing, but the accuracy cannot be the same as when the individual tree crown is seen on the orthophoto. The correlation in the riparian is the least as the trees are intermingled more than the medium and dense canopies. Also, the trees have different height resulting in some tree crowns partly visible in the orthophoto and canopy height model.

The result obtained contradict Shah (2011) who found a linear relationship between CPA and DBH of trees in the tropical forest. However, the result is similar to Shimano (1997) who also obtained a non-linear relationship between CPA and DBH. Shimano (1997) explained that while the DBH grows fast, the expansion of the tree crown is slow. The expansion of CPA will stabilize over time while the DBH of the tree will increase resulting in the non-linear relation.

#### **4.4. Comparison of UAV and field point estimated tree height**

The average tree height estimated indicates that the tree height estimated in the open, medium, and dense canopy from UAV, field points, and clinometer measured is almost the same resulting in the conclusion that there is statistically not a significant difference in the tree height estimated from UAV and field point CHM. This is because of the generation of good DTM due to the quality, quantity, and distribution of UAV generated points (Figure 4-3 and 4-4). The result is similar to Akindele (1991) whose model predicted the height of 9 and 11-year-old teak to be between 14 – 16 m.

The average height of trees in the riparian forest from the clinometer and field point CHM were almost the same (difference of about 0.3) but differs from tree height estimated by UAV CHM by about 4 m. The underestimation could be due to the difficulty of UAV images mirroring some part of the riparian forest resulting in no points generated in some section of the riparian (Figure 4-3). Since the age of the tree in the riparian forest is not known, it was impossible to compare with existing models.

#### **4.5. Aboveground carbon estimation**

Aboveground carbon was estimated using allometric equations developed by Polinder (2016) and Chave et al. (2014). Both equations use DBH and height of tree as input to estimate aboveground carbon. While Polinder (2016) equation was used for teak trees, Chave et al. (2014) was used for the trees in the riparian forest as it has trees of different DBH and height. From the allometric equation and the input parameters, aboveground carbon per tree was estimated.

The only variable that was different when estimating aboveground carbon is tree height (UAV and field). Tree height improves the estimation of aboveground carbon by about 5% (Feldpausch et al., 2011). Hence for tree height to influence aboveground carbon estimated, it needs to be significant. The height of trees estimated in the plantation forest from UAV was not significantly different to tree height estimated from field data. However, the tree height difference was significant when estimated from UAV and field data in the riparian forest and this could likely be because of the limitation of the UAV not mirroring forest floor in dense riparian forest.

Not all trees in the riparian forest were used to estimate aboveground carbon. Only the trees that were visible in the orthophoto were used and this would also influence the aboveground carbon estimated. From the individual UAV images, aboveground carbon of about 18% of the trees in the riparian were not estimated. However, this could be more as there could be some trees that were captured by the UAV images due to the dense canopy in the tropical forest.

The method used in this research is similar to the method used by Berhe (2018) and Odia (2018) who also derived forest parameters (DBH and tree height) from UAV data to estimate aboveground carbon. Although the method is similar, the method implemented in this study was able to relate the estimated aboveground carbon to the specific tree which was a limitation in the method implemented by Odia (2018) and Berhe (2018). The limitation to Odia (2018) and Berhe (2018) method was because handheld GPS, which has an accuracy of 3 to 10m in the forest, was used to record the coordinate of trees. Hence it was difficult to relate the estimated AGC to the specific tree as GPS point of trees sometimes does not lie within the boundary of the corresponding tree's crown projection area. Also, this method quantifies the DTM errors and the possible source of the error.

#### **4.6. Limitations**

The benchmark that was used to transfer the coordinates to the forest reserve was far. Although the survey instrument has a sub-meter accuracy, it is possible that accumulated error might affect the topographic survey. According to the instrument (Trimble R10) specification, the horizontal and vertical error per single RTK baseline (distance between base and rover) less than 30 Km is 8 mm ppm and 15 mm ppm respectively (Trimble, 2012). Seven benchmarks were established to transfer the coordinates from Offinso to the study area (Figure 2-4); hence the total accumulated error is 56 mm in the horizontal (east and north) and 105 mm in elevation.

The intermingling effect influences the crown projection area estimated. From the allometric equations used, DBH has more weight on the estimation of aboveground carbon than tree height. Hence the wrong estimation of DBH may influence the estimation of aboveground carbon especially in the riparian forest where tree crown intermingling is mostly observed.

Also, the allometric equation used for the riparian forest was not developed for Ghana although it was developed to estimate aboveground biomass for trees in the tropical forest. It would have been better to use allometric equation aboveground carbon (AGC) due to the difference in climate, topography, tree species, soil, and age (Basuki et al., 2009).

Furthermore, the method cannot quantify the number of trees that were missed in the riparian forest and this would lead to under estimation of aboveground carbon in the riparian forest.

## 5. CONCLUSION AND RECOMMENDATION

### 5.1. Conclusion

The study aimed to estimate the accuracy of DTM generated by UAV under different forest canopy density and evaluate its effect on the estimation of aboveground carbon. Various spatial and statistical analysis were executed to obtain forest parameters (DBH and tree height) which was used as input in an allometric equation to estimate aboveground biomass. A conversion factor was then used to estimate aboveground carbon. Based on the research questions and result from the analysis, the following conclusions were derived.

#### 5.1.1. What is the accuracy of DTM generated from UAV acquired images as compared to field point?

From the result, the root mean square error of the elevation in the open, medium, dense, and riparian forest are 1.05 m, 1.6 m, 1.7 m, and 3.8 m respectively. Since the RMSE increased with increasing canopy density, the null hypothesis was rejected.

#### 5.1.2. What is the relation between CPA and field measured DBH?

From the models developed, the quadratic model was used to predict DBH in the canopy density classes. The R-squared of the open, medium, dense, and the riparian forest canopy was estimated to be 0.9188, 0.8353, 0.8002, and 0.8252 respectively. From the model, there is a relation between CPA and DBH. Hence the null hypothesis was rejected.

#### 5.1.3. What is the difference in tree height generated from UAV and field point CHM?

From the canopy height model estimated, there is no statistical difference in tree height estimated from UAV and field point in the open, medium, and dense plantation canopy density. However, tree height estimated in the riparian forest from UAV and field data are statistically different. Hence the null hypothesis was not rejected for open, medium, and dense canopy but rejected for riparian forest.

#### 5.1.4. What is the difference in the aboveground carbon estimated from UAV dataset compared to field point?

According to the t-test, aboveground carbon estimated by UAV in open, medium, and dense plantation forest is not significantly different to aboveground carbon estimated from field point data. However, aboveground carbon estimated from UAV in the riparian forest is significantly different from aboveground carbon estimated field point. Hence the null hypothesis was not rejected for open, medium, and dense canopy but rejected for the riparian forest.

### 5.2. Recommendation

The type of data selected will affect the model development and validation process. For instance, when small and big trees are used for model development and validation respectively, the model developed will be different from using an equal number of big and small trees. Hence care must be taken when selecting the data for model CPA-DBH model development and validation.

Also, the amount of points generated in the dense canopy and riparian forest are different even though both forest canopies are dense. The riparian forest has a lower point density compared to the dense canopy plantation. One common difference is that unlike teak plantation, the riparian forest has many undergrowths and intermingling crown making the forest canopy denser. Therefore, I recommend research into the influence of leaf area index (LAI) on the quality of UAV DTM generated.

Finally, care must be taken when flying the UAV so the block for the UAV survey is not close to the boundary for the study to avoid edge effects. The lower part of Figure 3-3 contained a dense canopy class but could not be used because of edge effects which introduce error. The error is due to the fewer number of tie points at the edge hence reducing the quality of point cloud generated at the edge. To avoid this, the flight should be planned in such a way that the number of overlaps is at the edge of the UAV block is almost the same as the number of overlap at the middle of the UAV block (van Leeuwen, 2019).

## LIST OF REFERENCES

---

- Agisoft. (2018). Agisoft PhotoScan Professional user manual. Retrieved from [https://www.agisoft.com/pdf/photoscan-pro\\_1\\_4\\_en.pdf](https://www.agisoft.com/pdf/photoscan-pro_1_4_en.pdf)
- Akindele, S. O. (1991). Development of a site index equation for teak plantations in Southwestern Nigeria. *Journal of Tropical Forest Science*, 4(2), 162–169.
- Baccini, A., Goetz, S. J., Walker, W. S., Laporte, N. T., Sun, M., Sulla-Menashe, D., Hackler, J., Beck, P.S.A., Dubayah, R., Friedl, M.A., Samanta, S., & Houghton, R. A. (2012). Estimated carbon dioxide emissions from tropical deforestation improved by carbon-density maps. *Nature Publishing Group*, 2(1), 182–185. <https://doi.org/10.1038/NCLIMATE1354>
- Balenović, I., Marjanović, H., Paladinić, E., Zorana, M., & Sever, O. (2016). Quality assessment of high density digital surface model over different land cover classes. *Periodicum Biologorum*, 117(4), 459–470.
- Baral, S. (2011). Mapping carbon stock using high resolution satellite images in sub-tropical forest of Nepal (Master's thesis). University of Twente. Retrieved from [http://www.itc.nl/Pub/Home/library/Academic\\_output/AcademicOutput.html?p=11&y=11&l=20](http://www.itc.nl/Pub/Home/library/Academic_output/AcademicOutput.html?p=11&y=11&l=20)
- Basuki, T. M., van Laake, P. E., Skidmore, A. K., & Hussin, Y. A. (2009). Allometric equations for estimating the above-ground biomass in tropical lowland Dipterocarp forests. *Forest Ecology and Management*, 257(8), 1684–1694. <https://doi.org/10.1016/J.FORECO.2009.01.027>
- Berhe, T. H. (2018). Towards a UAV based standalone system for estimating and mapping aboveground biomass/carbon stock in Berkelah Tropical Rain Forest, Malaysia (Master's thesis). University of Twente. Retrieved from <https://www.itc.nl/library/research/academic-output/msc-theses/?query=berhe&year=2018>
- Blanc, L., Echard, M., Herault, B., Bonal, D., Marcon, E., Chave, J., & Baraloto, C. (2009). Dynamics of aboveground carbon stocks in a selectively logged tropical forest. *Ecological Applications*, 19(6), 1397–1404. <https://doi.org/10.1890/08-1572.1>
- Boisvenue, C., Smiley, B. P., White, J. C., Kurz, W. A., & Wulder, M. A. (2016). Integration of Landsat time series and field plots for forest productivity estimates in decision support models. *Forest Ecology and Management*, 376(1), 284–297. <https://doi.org/10.1016/j.foreco.2016.06.022>
- Böttcher, H., Eisbrenner, K., Fritz, S., Kindermann, G., Kraxner, F., McCallum, I., & Obersteiner, M. (2009). An assessment of monitoring requirements and costs of “Reduced Emissions from Deforestation and Degradation.” *Carbon Balance and Management*, 4(1), 1–14. <https://doi.org/10.1186/1750-0680-4-7>
- Brovkina, O., Novotny, J., Cienciala, E., Zemek, F., & Russ, R. (2017). Mapping forest aboveground biomass using airborne hyperspectral and LiDAR data in the mountainous conditions of Central Europe. *Ecological Engineering*, 100, 219–230. <https://doi.org/10.1016/J.ECOLENG.2016.12.004>
- By, R. de, Huisman, O., Knippers, R., Kraak, M.-J., & Stein, A. (2013). Spatial data modelling, collection and management. In *The core of GIScience* (pp. 237–312). Enschede.
- Cairns, M. A., Brown, S., Helmer, E. H., & Baumgardner, G. A. (1997). Root biomass allocation in the world's upland forests. *Oecologia*, 111(1), 1–11. <https://doi.org/10.1007/s004420050201>
- Castedo-Dorado, F., Gómez-García, E., Diéguez-Aranda, U., Barrio-Anta, M., & Crecente-Campo, F. (2012). Aboveground stand-level biomass estimation: A comparison of two methods for major forest species in northwest Spain. *Annals of Forest Science*, 69(6), 735–746. <https://doi.org/10.1007/s13595-012-0191-6>
- Chapman, A. (2019). Types of drones: multi-rotor vs fixed-wing vs single rotor vs hybrid VTOL. Retrieved December 30, 2018, from <https://www.auav.com.au/articles/drone-types/>
- Debella-Gilo, M. (2016). Bare-Earth extraction and DTM generation from photogrammetric point clouds with a partial use of an existing lower resolution DTM. *International Archives of the Photogrammetry, Remote Sensing and Spatial Information Sciences*, XLI, 201–206. <https://doi.org/10.5194/isprsarchives-XLI-B3-201-2016>
- Doane, D. P., & Seward, L. E. (2011). Measuring skewness: A forgotten statistic? *Journal of Statistics*, 19(2), 1–18. <https://doi.org/10.1080/10691898.2011.11889611>
- Ene, L. T., Næsset, E., Gobakken, T., Mauya, E. W., Bollandås, O. M., Gregoire, T. G., Ståhl, G., & Zahabu, E. (2016). Large-scale estimation of aboveground biomass in miombo woodlands using airborne laser scanning and national forest inventory data. *Remote Sensing of Environment*, 186, 626–636. <https://doi.org/10.1016/J.RSE.2016.09.006>
- ESA. (2012). Multipath. Retrieved September 10, 2018, from

- <https://gssc.esa.int/navipedia/index.php/Multipath>
- Esri. (2016a). Block adjustment for mosaic datasets. Retrieved February 1, 2019, from <http://desktop.arcgis.com/en/arcmap/10.3/manage-data/raster-and-images/block-adjustment-for-mosaic-datasets.htm>
- Esri. (2016b). Fundamentals of orthorectifying a raster dataset. Retrieved February 5, 2019, from <http://desktop.arcgis.com/en/arcmap/10.3/manage-data/raster-and-images/fundamentals-of-orthorectifying-a-raster-dataset.htm>
- Esri. (2016c). What is a TIN surface? Retrieved January 28, 2019, from <http://desktop.arcgis.com/en/arcmap/10.3/manage-data/tin/fundamentals-of-tin-surfaces.htm>
- Esri. (2018). How inverse distance weighted interpolation works. Retrieved January 28, 2019, from <http://pro.arcgis.com/en/pro-app/help/analysis/geostatistical-analyst/how-inverse-distance-weighted-interpolation-works.htm>
- Ferraz, A., Saatchi, S., Mallet, C., & Meyer, V. (2016). LiDAR detection of individual tree size in tropical forests. *Remote Sensing of Environment*, 183, 318–333. <https://doi.org/10.1016/j.rse.2016.05.028>
- Ford, C. (2015). Understanding Q-Q Plots. Retrieved February 11, 2019, from <https://data.library.virginia.edu/understanding-q-q-plots/>
- Fras, M. K., Kerin, A., Mesarič, M., Peterman, V., & Grigillo, D. (2016). Assessment of the quality of Digital Terrain Model produced from Unmanned Aerial System imagery. *International Archives of the Photogrammetry, Remote Sensing and Spatial Information Sciences - ISPRS Archives*, 41(23), 893–899. <https://doi.org/10.5194/isprsarchives-XLI-B1-893-2016>
- Getzin, S., Wiegand, K., & Schöning, I. (2012). Assessing biodiversity in forests using very high-resolution images and unmanned aerial vehicles. *Methods in Ecology and Evolution*, 3(2), 397–404. <https://doi.org/10.1111/j.2041-210X.2011.00158.x>
- Gibbs, H. K., Brown, S., Niles, J. O., & Foley, J. A. (2007). Monitoring and estimating tropical forest carbon stocks: Making REDD a reality. *Environmental Research Letters*, 2(4). <https://doi.org/10.1088/1748-9326/2/4/045023>
- Gomes, M. F., & Maillard, P. (2016). Detection of tree crowns in very high spatial resolution images. In *Environmental Applications of Remote Sensing*. InTech. <https://doi.org/10.5772/62122>
- Grace, J., Mitchard, E., & Gloor, E. (2014). Perturbations in the carbon budget of the tropics. *Global Change Biology*, 20(10), 3238–3255. <https://doi.org/10.1111/gcb.12600>
- Graham, V., Laurance, S. G., Grech, A., & Venter, O. (2017). Spatially explicit estimates of forest carbon emissions, mitigation costs and REDD+ opportunities in Indonesia. *Environmental Research Letters*, 12(4). <https://doi.org/10.1088/1748-9326/aa6656>
- Hexagon Positional System. (n.d.). Section 1: An introduction to GNSS. Retrieved September 9, 2018, from <https://www.novatel.com/an-introduction-to-gnss/chapter-1-gnss-overview/section-1/>
- Hirata, Y., Tsubota, Y., & Sakai, A. (2009). Allometric models of DBH and crown area derived from QuickBird panchromatic data in *Cryptomeria japonica* and *Chamaecyparis obtusa* stands. *International Journal of Remote Sensing*, 30(19), 5071–5088. <https://doi.org/10.1080/01431160903022977>
- Hosseinyalamdary, S. (2018). Positioning Technologies [Lecture note]. Retrieved from [https://blackboard.utwente.nl/bbcswebdav/pid-1159096-dt-content-rid-3142841\\_2/courses/M18-EOS-103/positioning technologies.pdf](https://blackboard.utwente.nl/bbcswebdav/pid-1159096-dt-content-rid-3142841_2/courses/M18-EOS-103/positioning%20technologies.pdf)
- Hussin, Y. A. (2018). What is Biomass and carbon? [Lecture note] Retrieved from [https://blackboard.utwente.nl/bbcswebdav/pid-1157389-dt-content-rid-3113189\\_2/courses/M18-NRS-100/What is biomass and carbon%281%29.pdf](https://blackboard.utwente.nl/bbcswebdav/pid-1157389-dt-content-rid-3113189_2/courses/M18-NRS-100/What%20is%20biomass%20and%20carbon%281%29.pdf)
- Hyypä, J., Holopainen, M., Olsson, H., Hyypä, J., Holopainen, M., & Olsson, H. (2012). Laser scanning in Forests. *Remote Sensing*, 4(10), 2919–2922. <https://doi.org/10.3390/rs4102919>
- Ioki, K., Tsuyuki, S., Hirata, Y., Phua, M.-H., Wong, W. V. C., Ling, Z.-Y., Saito, H., & Takao, G. (2014). Estimating above-ground biomass of Tropical rainforest of different degradation levels in Northern Borneo using airborne LiDAR. *Forest Ecology and Management*, 328, 335–341. <https://doi.org/10.1016/J.FORECO.2014.06.003>
- IPCC. (2013). *Climate Change 2013: The Physical Science basis*. Retrieved February 5, 2019, from <https://www.ipcc.ch/report/ar5/wg1/>
- Jung, S.-E., Kwak, D.-A., Park, T., Lee, W.-K., Yoo, S., Jung, S.-E., Kwak, D.-A., Park, T., Lee, W.-K., & Yoo, S. (2011). Estimating Crown Variables of Individual Trees Using Airborne and Terrestrial Laser Scanners. *Remote Sensing*, 3(11), 2346–2363. <https://doi.org/10.3390/rs3112346>

- Kankare, V., Holopainen, M., Vastaranta, M., Puttonen, E., Yu, X., Hyyppä, J., Vaaja, M., Hyyppä, H., & Alho, P. (2013). Individual tree biomass estimation using terrestrial laser scanning. *ISPRS Journal of Photogrammetry and Remote Sensing*, 75, 64–75. <https://doi.org/10.1016/j.isprsjprs.2012.10.003>
- Kaosa-ard, A. (1995). Management of Teak plantations. Retrieved February 1, 2019, from <http://www.fao.org/docrep/005/AC773E/ac773e08.htm#TopOfPage>
- Kauranne, T., Joshi, A., Gautam, B., Manandhar, U., Nepal, S., Peuhkurinen, J., Hämäläinen, J., Junntila, V., Gunia, K., Latva-Käyrä, P., Kolesnikov, A., & Leppänen, V. (2017). LiDAR-Assisted Multi-Source Program (LAMP) for measuring above ground biomass and forest carbon. *Remote Sensing*, 9(2), 1–36. <https://doi.org/10.3390/rs9020154>
- Knippers, R., & Tempfli, K. (2012). Spatial referencing and satellite-based positioning. In *The Core of GIScience* (pp. 93–125). Enschede. <https://doi.org/10.1016/B978-0-12-385889-4.00013-2>
- Li, J., & Heap, A. D. (2008). A Review of Spatial Interpolation Methods for Environmental Scientists. Australia. Retrieved from <https://pdfs.semanticscholar.org/686c/29a81eab59d7f6b7e2c4b060b1184323a122.pdf>
- Lisein, J., Pierrot-deseilligny, M., Lejeune, P., & Management, N. (2013). A photogrammetric workflow for the creation of a forest canopy height model from Small Unmanned Aerial System Imagery. *Forests*, 4, 922–944. <https://doi.org/10.3390/f4040922>
- Luoma, V., Saarinen, N., Wulder, M. A., White, J. C., Vastaranta, M., Holopainen, M., & Hyyppä, J. (2017). Assessing precision in conventional field measurements of individual tree attributes. *Forests*, 8(2), 1–16. <https://doi.org/10.3390/f8020038>
- Malhi, Y. (2010). The carbon balance of Tropical forest regions, 1990–2005. *Current Opinion in Environmental Sustainability*, 2(4), 237–244. <https://doi.org/10.1016/J.COSUST.2010.08.002>
- MathWorks. (2018). Structure from Motion. Retrieved September 10, 2018, from <https://nl.mathworks.com/help/vision/ug/structure-from-motion.html>
- Messinger, M., Asner, G., Silman, M., Messinger, M., Asner, G. P., & Silman, M. (2016). Rapid assessments of Amazon forest structure and biomass using small Unmanned Aerial Systems. *Remote Sensing*, 8(8), 1-15. <https://doi.org/10.3390/rs8080615>
- Mohren, G., Hasenauer, H., Köhl, M., & Nabuurs, G.-J. (2012). Forest inventories for carbon change assessments. *Current Opinion in Environmental Sustainability*, 4(6), 686–695. <https://doi.org/10.1016/j.cosust.2012.10.002>
- Nagelkerke, N. J. D. (2008). A note on a general definition of the coefficient of determination. *Biometrika*, 78(3), 691-692. <https://doi.org/10.2307/2337038>
- NASA. (2018). The consequences of climate change. Retrieved July 1, 2018, from <https://climate.nasa.gov/effects/>
- Nex, F. (2018a). Unmanned Aerial Vehicles for Earth Observation. Enschede. Retrieved from [https://blackboard.utwente.nl/bbcswebdav/pid-1157640-dt-content-rid-3116822\\_2/courses/M18-EOS-103/Reader\\_M13\\_2018.pdf](https://blackboard.utwente.nl/bbcswebdav/pid-1157640-dt-content-rid-3116822_2/courses/M18-EOS-103/Reader_M13_2018.pdf)
- Nex, F. (2018b). Unmanned Aerial Vehicles for Earth Observation and ESE applications. Last updated 20 December 2016 (1st ed.). Retrieved from <http://www.ncl.ac.uk/ceser/research/observation/uav-ese-applications/%5Cnhttp://www.ncl.ac.uk/ceser/researchprogramme/observationmonitoring/uavsforeseapplications/>
- Odia, B. E. (2018). Unmanned Aerial Vehicle (UAV) Datasets for retrieval of Forest parameters and estimation of aboveground biomass in Berkelah Tropical Rainforest, Malaysia (Master's thesis). University of Twente. <https://library-itc-utwente-nl.ezproxy2.utwente.nl/login/2018/msc/nrm/odia.pdf>
- Ota, T., Ogawa, M., Shimizu, K., Kajisa, T., Mizoue, N., & Yoshida, S., (2015). Aboveground biomass estimation using Structure from Motion approach with aerial photographs in a seasonal Tropical forest. *Forests*, 6, 3882–3898. <https://doi.org/10.3390/f6113882>
- Ounban, W., Puangchit, L., & Diloksumpun, S. (2016). Development of general biomass allometric equations for *Tectona grandis* and *Eucalyptus camaldulensis* Dehnh plantations in Thailand. *Agriculture and Natural Resources*, 50(1), 48–53. <https://doi.org/10.1016/J.ANRES.2015.08.001>
- Peltoniemi, M., Palosuo, T., Monni, S., & Mäkipää, R. (2006). Factors affecting the uncertainty of sinks and stocks of carbon in Finnish forests soils and vegetation. *Forest Ecology and Management*, 232(1–3), 75–85. <https://doi.org/10.1016/J.FORECO.2006.05.045>
- Pirotti, F. (2011). Analysis of full-waveform LiDAR data for forestry applications: A review of investigations and methods. *Iforest*, 4(3), 100-106. <https://doi.org/10.3832/IFOR0562-004>
- Pix4D. (2018a). Before starting a project: Designing the image acquisition plan. Retrieved September 12, 2018,



- from <https://support.pix4d.com/hc/en-us/articles/202557409-Step-1-Before-Starting-a-Project-1-Designing-the-Image-Acquisition-Plan>
- Pix4D. (2018b). Menu process: Processing options. Retrieved November 12, 2018, from <https://support.pix4d.com/hc/en-us/articles/202557769#label5>
- Pix4D. (2018c). Quality report. Retrieved November 5, 2018, from <https://support.pix4d.com/hc/en-us/articles/202558689-Quality-Report-Help#label7>
- Pix4D. (2018d). What affects the quality of the DSM? Retrieved November 5, 2018, from <https://support.pix4d.com/hc/en-us/articles/202558779-What-affects-the-Quality-of-the-DSM-PrecisionHawk>.
- PrecisionHawk. (2018). Sensors 101: The basics of LiDAR, thermal, hyperspectral, and multispectral technology. Retrieved December 30, 2018, from <https://www.precisionhawk.com/media/topic/sensors-101-basics-lidar-thermal-hyperspectral-multispectral-technology/>
- Radío, M. I. L., & Delgado, D. M. (2014). Management of young teak plantations in Panama - Effect of pruning and thinning (Master's thesis). Swedish University of Agricultural Sciences. Retrieved from <http://stud.epsilon.slu.se/7279/>
- Rodríguez-Veiga, P., Wheeler, J., Louis, V., Tansey, K., & Balzter, H. (2017). Quantifying forest biomass carbon stocks from space. *Current Forestry Reports*, 3(1), 1–18. <https://doi.org/10.1007/s40725-017-0052-5>
- Saatchi, S. S., Harris, N. L., Brown, S., Lefsky, M., Mitchard, E. T. A., Salas, W., Zutta, B.R., Buermann, W., Lewis, S.L., Hagen, S., Petrova, S., White, L., Silman, M., & Morel, A. (2011). Benchmark map of forest carbon stocks in tropical regions across three continents. *Proceedings of the National Academy of Sciences of the United States of America*, 108(24), 9899–904. <https://doi.org/10.1073/pnas.1019576108>
- Scheidel, A., & Work, C. (2018). Forest plantations and climate change discourses: New powers of ‘green’ grabbing in Cambodia. *Land Use Policy*, 77, 9–18. Retrieved from <https://doi.org/10.1016/j.landusepol.2018.04.057>
- Shah, S. K. (2011). Modelling the relationship between tree canopy projection area and above ground carbon stock using high resolution Geoeye satellite images (Master's thesis). University of Twente. [https://webapps.itc.utwente.nl/librarywww/papers\\_2011/msc/nrm/shah.pdf](https://webapps.itc.utwente.nl/librarywww/papers_2011/msc/nrm/shah.pdf)
- Shahbazi, M., Théau, J., & Ménard, P. (2014). Recent applications of unmanned aerial imagery in Natural Resource Management. *GIScience & Remote Sensing*, 51(4), 339–365. <https://doi.org/10.1080/15481603.2014.926650>
- Shimano, K. (1997). Analysis of the Relationship between DBH and Crown Projection Area Using a New Model. *Journal of Forest Research*, 2(4), 237–242. <https://doi.org/10.1007/BF02348322>
- Snaveley, N., Seitz, S. M., & Szeliski, R. (2008). Modeling the World from Internet Photo Collections. *International Journal of Computer Vision*, 80(2), 189–210. <https://doi.org/10.1007/s11263-007-0107-3>
- Song, C., Dickinson, M. B., Su, L., Zhang, S., & Yaussey, D. (2010). Estimating average tree crown size using spatial information from Ikonos and QuickBird images: Across-sensor and across-site comparisons. *Remote Sensing of Environment*, 114(5), 1099–1107. <https://doi.org/10.1016/J.RSE.2009.12.022>
- Tan, Q., & Xu, X. (2014). Comparative analysis of spatial interpolation methods: An experimental study. *Sensors and Transducers*, 165(2), 155–163. <https://doi.org/http://dx.doi.org/10.3928/00904481-20100521-09>
- Tomašík, J., Mokroš, M., Saloš, S., Chudý, F., & Tuňák, D. (2017). Accuracy of photogrammetric UAV-based point clouds under conditions of partially-open forest canopy. *Forests*, 8(5), 221–227. <https://doi.org/10.3390/f8050151>
- Trimble. (2012). Trimble R10 GNSS System. Retrieved September 9, 2018, from [https://www.trimble.com/Survey/Trimble-R10.aspx?tab=GNSS\\_System\\_Comparison](https://www.trimble.com/Survey/Trimble-R10.aspx?tab=GNSS_System_Comparison)
- Trimble. (2014). User guide-Trimble R10 GNSS receiver. Retrieved September 8, 2018, from <https://docplayer.net/54591354-User-guide-trimble-r10-gnss-receiver.html>
- Trimble. (2018). Trimble - GPS Tutorial. Retrieved September 9, 2018, from [https://www.trimble.com/gps\\_tutorial/howgps-error2.aspx](https://www.trimble.com/gps_tutorial/howgps-error2.aspx)
- Turner, D., Lucieer, A., Watson, C., Turner, D., Lucieer, A., & Watson, C. (2012). An automated technique for generating georectified mosaics from ultra-high resolution Unmanned Aerial Vehicle (UAV) Imagery based on Structure from Motion (SfM) point clouds. *Remote Sensing*, 4(5), 1392–1410. <https://doi.org/10.3390/rs4051392>
- UNFCCC. (2018). Kyoto protocol - Targets for the first commitment period. Retrieved February 5, 2019, from <https://unfccc.int/process/the-kyoto-protocol>
- van Leeuwen, L. (2019). Flight plan [Audio recording]. Enschede.
- Wallace, L., Lucieer, A., Malenovsky, Z., Turner, D., & Vopěnka, P. (2016). Assessment of forest structure using

- two UAV techniques: A comparison of airborne laser scanning and structure from motion (SfM) point clouds. *Forests*, 7(3), 1–16. <https://doi.org/10.3390/f7030062>
- Wanders, T., & Tollenaar, M. (2017). Forest management plan - Asubima and Afrensu Brohuma forest reserves Ashanti Region, Ghana. Retrieved from [www.forinternational.nl](http://www.forinternational.nl)
- Westoby, M. J., Brasington, J., Glasser, N. F., Hambrey, M. J., & Reynolds, J. M. (2012). 'Structure-from-Motion' photogrammetry: A low-cost, effective tool for geoscience applications. *Geomorphology*, 179, 300–314. <https://doi.org/10.1016/J.GEOMORPH.2012.08.021>
- WyDOT, (2008). Measurements and errors. Retrieved October 1, 2018, from <https://doi.org/10.1002/dvg.22995>
- Yuen, J. Q., Fung, T., & Ziegler, A. D. (2016). Review of allometric equations for major land covers in South-Eastern Asia: Uncertainty and implications for above- and below-ground carbon estimates. *Forest Ecology and Management*, 360, 323–340. <https://doi.org/10.1016/J.FORECO.2015.09.016>
- Zaki, N. A. M., Latif, Z. A., Suratman, M. N., & Zainal, M. Z. (2016). Modelling the carbon stocks estimation of the Tropical lowland Dipterocarp forest using Lidar and remotely sensed data. *ISPRS Annals of Photogrammetry, Remote Sensing and Spatial Information Sciences*, III(7), 187–194. <https://doi.org/10.5194/isprsannals-III-7-187-2016>

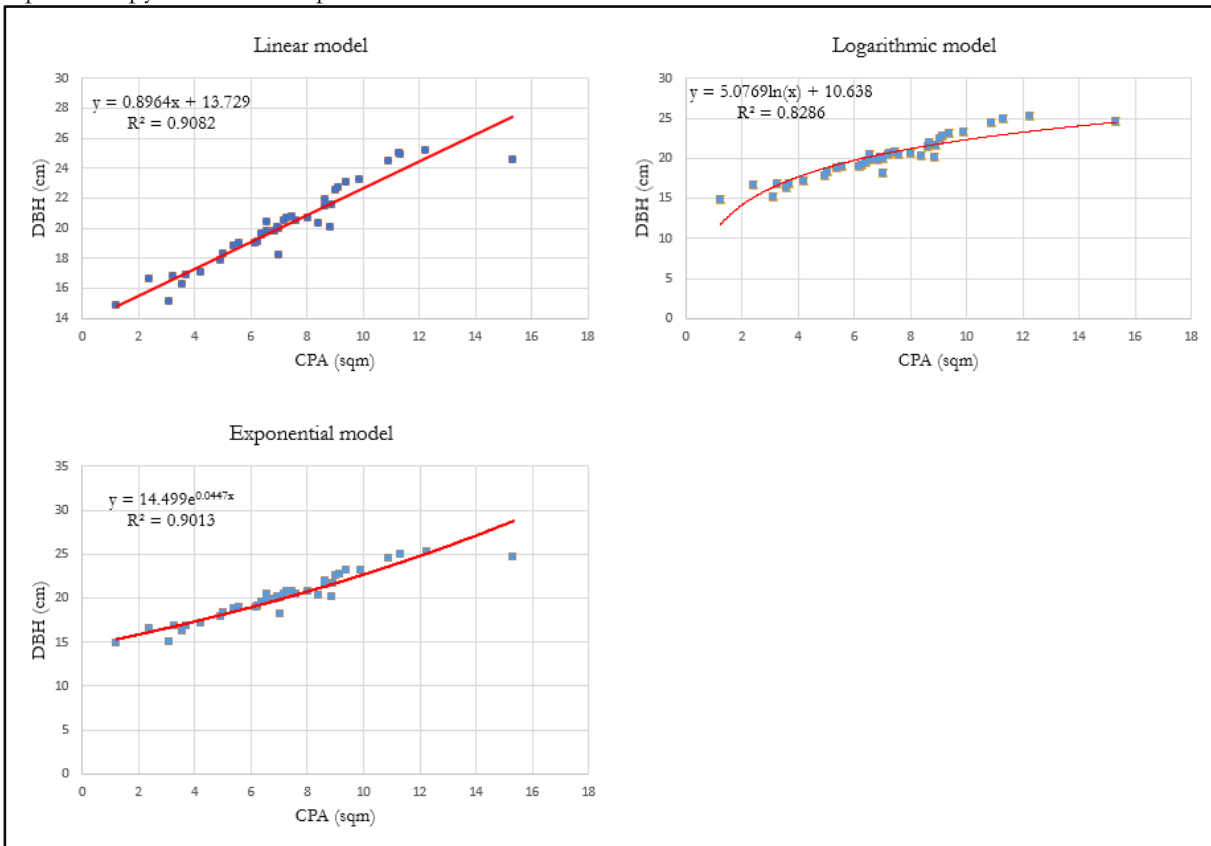
## 6. APPENDICES

Appendix 1: Field data collection sheet

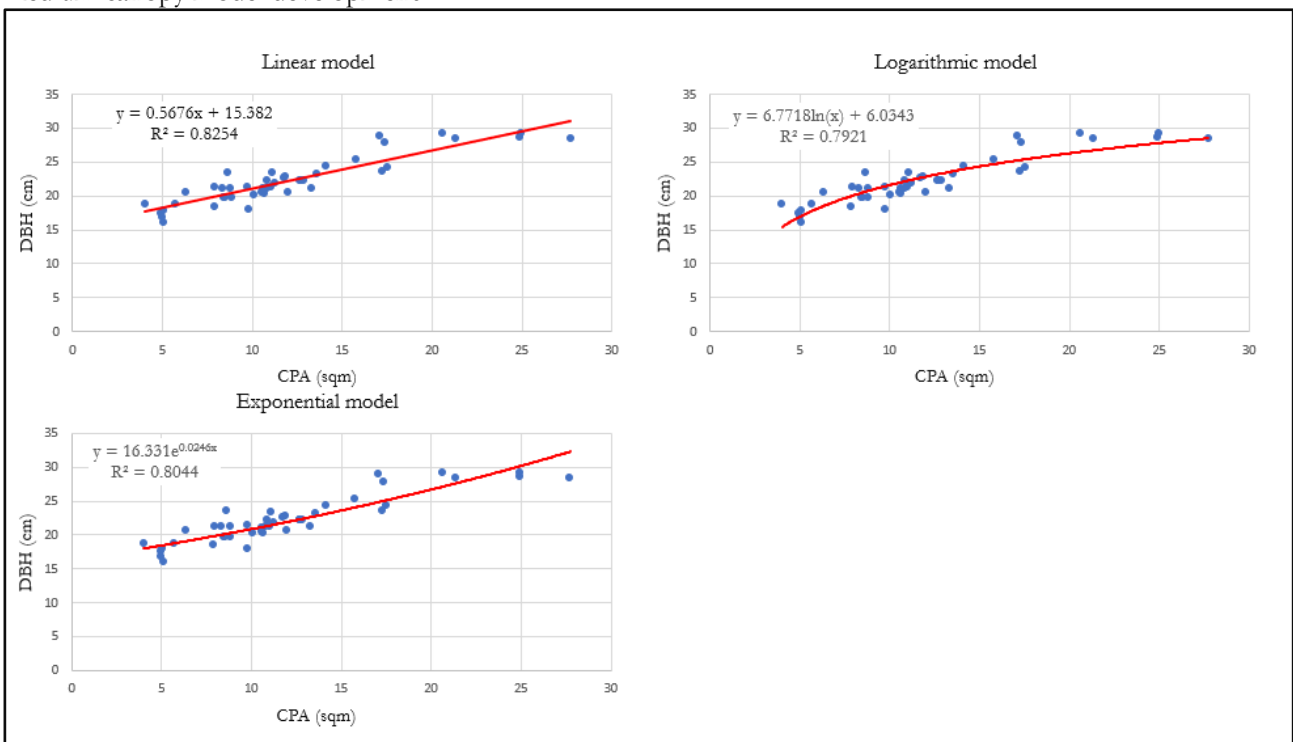
FIELD DATA COLLECTION SHEET				
Date			Canopy class:	
ID	DBH	Height	Species	Remarks

Appendix 2: DBH-CPA models

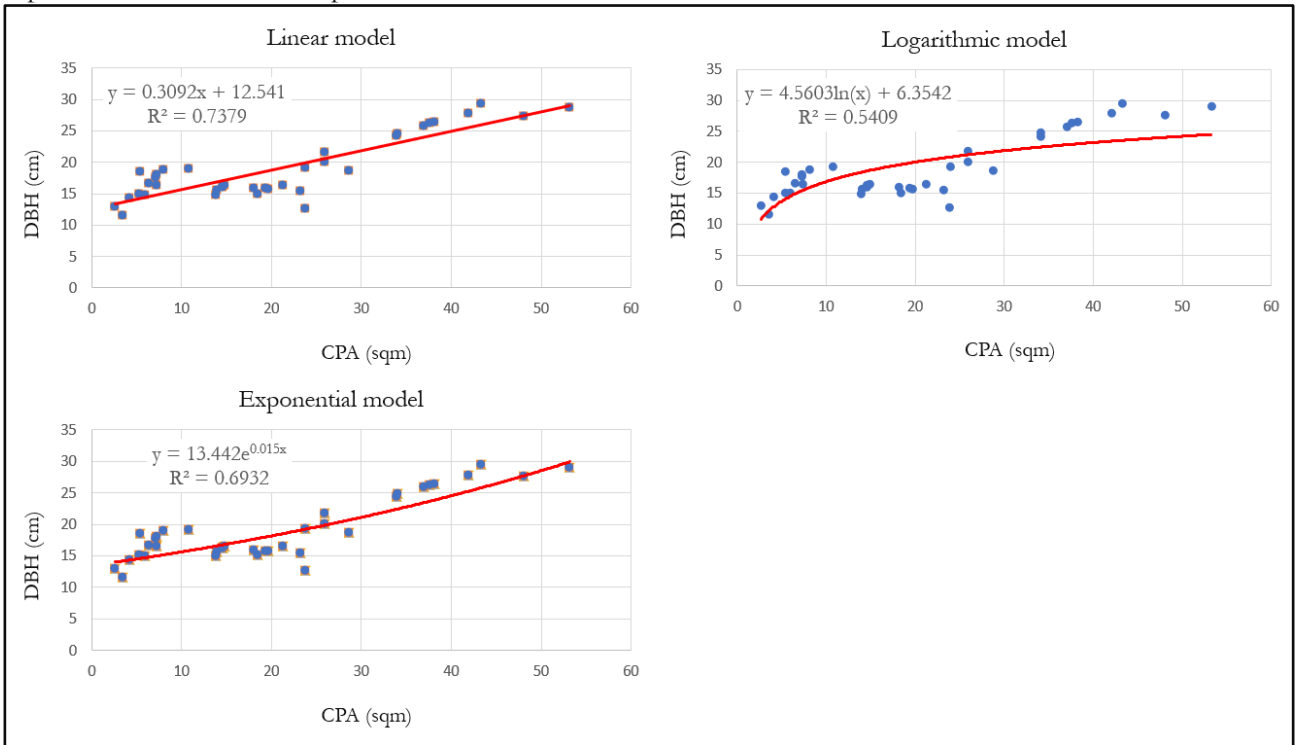
Open canopy model development



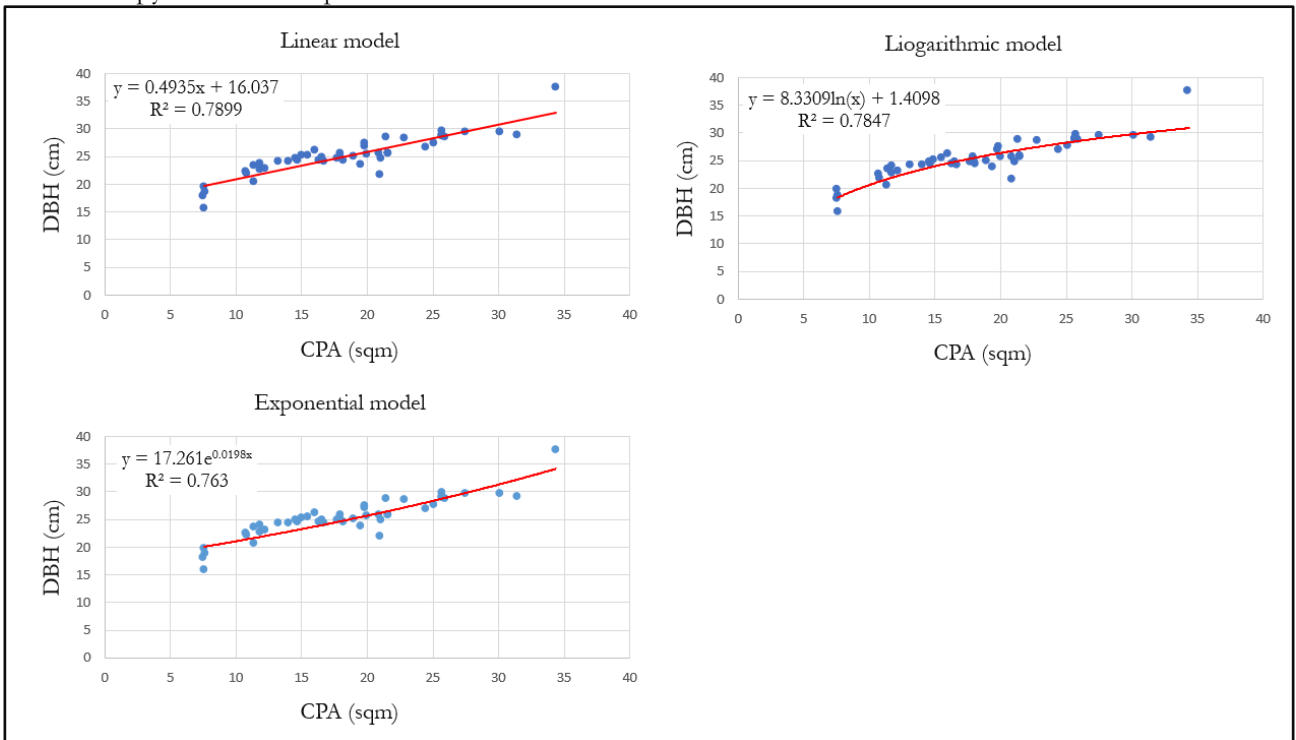
Medium canopy model development



Riparian forest model development



Dense canopy model development



### Appendix 3: Python code

```
import PhotoScan

chunk = PhotoScan.app.document.chunk
point_cloud = chunk.point_cloud
projections = point_cloud.projections
points = point_cloud.points
npoints = len(points)
tracks = point_cloud.tracks

THRESHOLD = 5

for camera in chunk.cameras:
    center = PhotoScan.Vector([camera.sensor.width/2, camera.sensor.height/2])

    point_index = 0
    for proj in projections[camera]:
        track_id = proj.track_id
        if (proj.coord - center).norm() > THRESHOLD:
            while point_index < npoints and points[point_index].track_id < track_id:
                point_index += 1
            if point_index < npoints and points[point_index].track_id == track_id:
                if not points[point_index].valid:
                    continue

            points[point_index].valid = False

print("Finished")
```